CIAMTIS

U.S. DOT Region 3 University Transportation Center

Laboratory Tests on Scaled Steel Fin Pile Foundations

April 9, 2021

Prepared by:

S. Prabhu, P. Te, T. Qiu, and J.A. Laman

The Pennsylvania State University

r3utc.psu.edu

PennState College of Engineering

LARSON TRANSPORTATION INSTITUTE

DISCLAIMER

Technical Report Documentation Page

1. Report No.	2. Government Accession No.	3. Recipient's Catalog No.
CIAM-UTC-REG09		

4. Title and Subtitle	5. Report Date
Laboratory Tests on Scaled Steel Fin Pile Foundations	April 9, 2021
	6. Performing Organization Code

7. Author(s)	8. Performing Organization Report No.
S. Prabhu, P. Te, T. Qiu, and J.A. Laman	LTI 2021-12

9. Performing Organization Name and Address	10. Work Unit No. (TRAIS)
The Thomas D Larson Pennsylvania Transportation Institute The Pennsylvania State University 201 Transportation Research Building University Park, PA 16802	11. Contract or Grant No. 69A3551847103

12. Sponsoring Agency Name and Address	13. Type of Report and Period Covered
U.S. Department of Transportation Research and Innovative Technology Administration 3rd Fl, East Bldg E33-461 1200 New Jersey Ave, SE Washington, DC 20590	Final Report 03/01/2021 – 04/09/2021
	14. Sponsoring Agency Code

15. Supplementary Notes

Work funded through The Pennsylvania State University through the University Transportation Center Grant Agreement, Grant No. 69A3551847103.

16. Abstract

The use of steel fin pile foundations (SFPFs) for offshore structures and their efficiency in increasing the lateral load capacity compared to unfinned piles has been extensively studied. Recently, SFPFs were introduced in the field of transportation engineering for supporting structures including signs, signals, etc. In these applications, foundations are subjected to torsional and combined torsion and lateral loads. However, the specification, construction, and application of SFPFs have been limited in these applications due to a lack of rigorous and detailed studies, especially under torsional and combined torsional and lateral loadings. In the present study, small-scale laboratory tests were carried out to evaluate the improvement in torsional and lateral load-carrying capacities of steel pipe piles by adding steel plates (fins) at grade level compared to the unfinned piles. The study also discusses the effect of arm length on the torsional and lateral load capacity during the combined torsional and lateral loading of SFPFs, as well as the zone/area of influence during the lateral pile loading for unfinned piles and SFPFs. Subsequently, combined torsional and lateral load tests were carried out on SFPFs with different moment arms to study the influence of arm length on the torsional and lateral load capacities. The laboratory studies, among other findings, showed that the introduction of fins significantly increases the torsional and lateral load capacities of monopiles, and that the torsional and lateral load capacities of both monopiles and SFPFs increase with an increase in sand density.

17. Key Words	18. Distribution Statement
Steel fin pile foundations, steel pipe, torsional and lateral loading, load-carrying capacity, moment arm	No restrictions. This document is available from the National Technical Information Service, Springfield, VA 22161

19. Security Classif. (of this report)	20. Security Classif. (of this page)	21. No. of Pages	22. Price
Unclassified	Unclassified	71	

Table of Contents

List of Figures

List of Tables

CHAPTER 1

Introduction

1.1 INTRODUCTION

Steel fin pile foundations (SFPFs) are an innovate pile design that improves the load-carrying capacity of steel pipe piles. SFPFs have been used extensively to support offshore structures (e.g., wind turbines) where the primary force is lateral loading. Recently, SFPFs have been utilized for transportation structures to support traffic signs and signal structures, which are subjected to lateral and torsional loads due to structure geometry and load eccentricity. The present study sought to understand and quantify the effectiveness of SFPFs against the action of lateral, torsional, and a combination of both loadings in comparison to unfinned pile foundations. The present study also sought to understand the influence zone of the SFPF and unfinned pile during lateral loading. The laboratory tests conducted generated data to facilitate the development of guidelines for the installation of SFPFs in the field for maximum efficiency.

1.2 BACKGROUND

Transportation structures, including signals and signposts, are subjected to wind loads. The eccentricity of the wind load subjects the supporting piles to translational load and rotational moments. The rotational resistance/torsional capacity of unfinned piles is commonly increased either by increasing the soil density surrounding the pile or by increasing the pile diameter and length. However, both solutions will increase project cost. An innovative solution for increasing both lateral load resistance and torsional resistance is to add steel plates, or fins, to the piles at four equally spaced positions. Piles with fins, heretofore referred to as SFPFs, compare favorably to traditional foundation systems and offer added efficiencies related to time, personnel, equipment, and worksite safety. However, the specification and construction of SFPFs has been limited due to a lack of rigorous and detailed SFPF studies. There are several published studies and guidelines for the design of unfinned piles; however, no experimental, analytical, or numerical studies are reported in the literature that provide insights into torsional capacity and combined torsional plus lateral load capacity of SFPFs. There is also a lack of understanding of the influence zone of the SFPFs during lateral loading.

1.3 PROBLEM STATEMENT

Numerical simulation is a powerful tool that enables understanding of SFPF performance. However, numerical models must be accurately calibrated against experimental or field data for the simulations to be valid. The effect of sand density on SFPF torsional and lateral load capacities must be studied. A direct comparison of torsional and lateral load resistance between unfinned pile and SFPF is necessary to understand the effectiveness of SFPFs. Studies have shown that the introduction of loading eccentricity reduces the torsional and lateral load capacities of unfinned piles. The present study tries to understand the effect of loading eccentricity on the torsional and lateral load capacity of SFPF by carrying out combined torsional and lateral load tests on SFPFs. Overall, the present study provides much-needed data for calibrating numerical models that will further enhance understanding of the effectiveness of SFPFs.

1.4 SCOPE AND OBJECTIVES

In the present study, 16 scaled laboratory tests were conducted on SFPFs and unfinned piles. It is noted in published studies that SFPFs are more effective in granular soils as compared to clayey soils. Due to the lack of torsional test data available in the literature, the laboratory tests on torsional loading are carried out in dry sand at three density ranges (D_r) of 20-30%, 45-55%, and 75-85%, typical for loose, medium dense, and dense sand, respectively. Tests on lateral loadings are carried out in medium dense and dense sand to understand the effect of density on the lateral load capacity and influence zone of SFPFs and unfinned piles. The combined lateral and torsional capacity tests are carried out in dry sands prepared at 45-55% and 75-85% relative densities. The pile length to diameter ratio ($L_p/D_p = 9$), fin width to pile diameter ($W_F/D_P = 1$), and fin configuration (four-fin configuration) of the SFPF used are constant for the present study and were determined on the basis of a careful review of the published literature.

The objective of the present study was to understand the effectiveness of SFPFs subjected to torsional loading, lateral loading, and a combination of both loadings as compared to unfinned piles. The torsional capacities of the SFPFs were compared with the unfinned piles to understand their performance at three different soil densities. The lateral load capacities including the influence zone of the SFPFs were also compared with unfinned piles at two soil densities. The reduction in lateral load capacity due to the introduction of a torsional arm in the SFPF was also studied by carrying out combined lateral and torsional load tests with different load eccentricities. Finally, guidelines were developed for the effective usage of SFPFs and unfinned piles in the field.

1.5 REPORT ORGANIZATION

Chapter 1 - Introduction: This chapter presents the background of this research and identifies the need for a better understanding of the behavior of SFPFs and unfinned piles for applications in the transportation sector. The justification of conducting the proposed laboratory experiments on SFPF and unfinned piles is also presented.

Chapter 2 - Literature Review: This chapter presents a detailed literature review of the experiments and field studies on unfinned piles and highlights the lack of torsional studies and the conventional lateral load tests on SFPFs. This chapter also discusses the lateral load tests on SFPFs and unfinned piles reported in the literature. The optimum fin pile geometry based on the lateral load test is discussed in detail.

Chapter 3 - Scaled Laboratory Study: A detailed explanation of the pile geometry and fin dimensions used for the study is discussed. This chapter also illustrates the pile specimens, fixtures, processes, materials, data acquisition system, and data processing used.

Chapter 4 - Experimental Test Results: The results of all laboratory tests are presented. The SFPF and unfinned pile results are compared in terms of torsional capacity, lateral load capacity, etc.

Chapter 5 - Findings: This chapter presents the summary and conclusions of this study.

Chapter 6 - Recommendations: This chapter presents recommendations for future study.

CHAPTER 2

Literature Review

2.1 INTRODUCTION

In this chapter, studies on shafts and unfinned piles under torsional, lateral, and a combination of both loadings are synthesized based on a literature review. Laboratory and field tests reported in the literature are reviewed to obtain control parameters for the present study. Based on the literature review, the control factors chosen for the present study are soil density for the lateral and torsional load tests on SFPFs and unfinned piles and arm length for the combined torsional and lateral load tests on SFPFs. The reduction in lateral load capacity by the introduction of torsional loadings in shafts is also discussed in detail. The performance of SFPFs and unfinned piles is discussed in terms of torque versus angular rotation for torsional load applications. For combined torsional and lateral load tests, the performance is discussed by noting torque versus angular rotation and lateral load versus lateral displacement. Only tests on unfinned piles are reported for the torsional and combined torsional and lateral load tests in this section, as the authors could not find any reliable studies on the torsional capacity of SFPFs.

2.2 TORSIONAL RESISTANCE STUDIES ON UNFINNED PILE

2.2.1 Laboratory Studies on Unfinned Pile Foundations

Initial studies on the torsional capacity of unfinned pile foundation were carried out by Poulos (1975). Poulos (1975) applied torsional load on four solid aluminum pipes driven into kaolin clay. Two piles with diameters of 25.4 mm (1 in.) and 19 mm (0.75 in.) were used and for each pipe diameter, two lengths of 502 mm (20 in.) and 254 mm (10 in.) were tested. Results were reported in terms of torque applied (τ) versus angular rotation (θ) as shown in Figure 2.1. Poulos (1975) noted that torque did not achieve a definitive peak for the angular rotation considered; however, the increase in torque magnitude decreased at very high θ values.

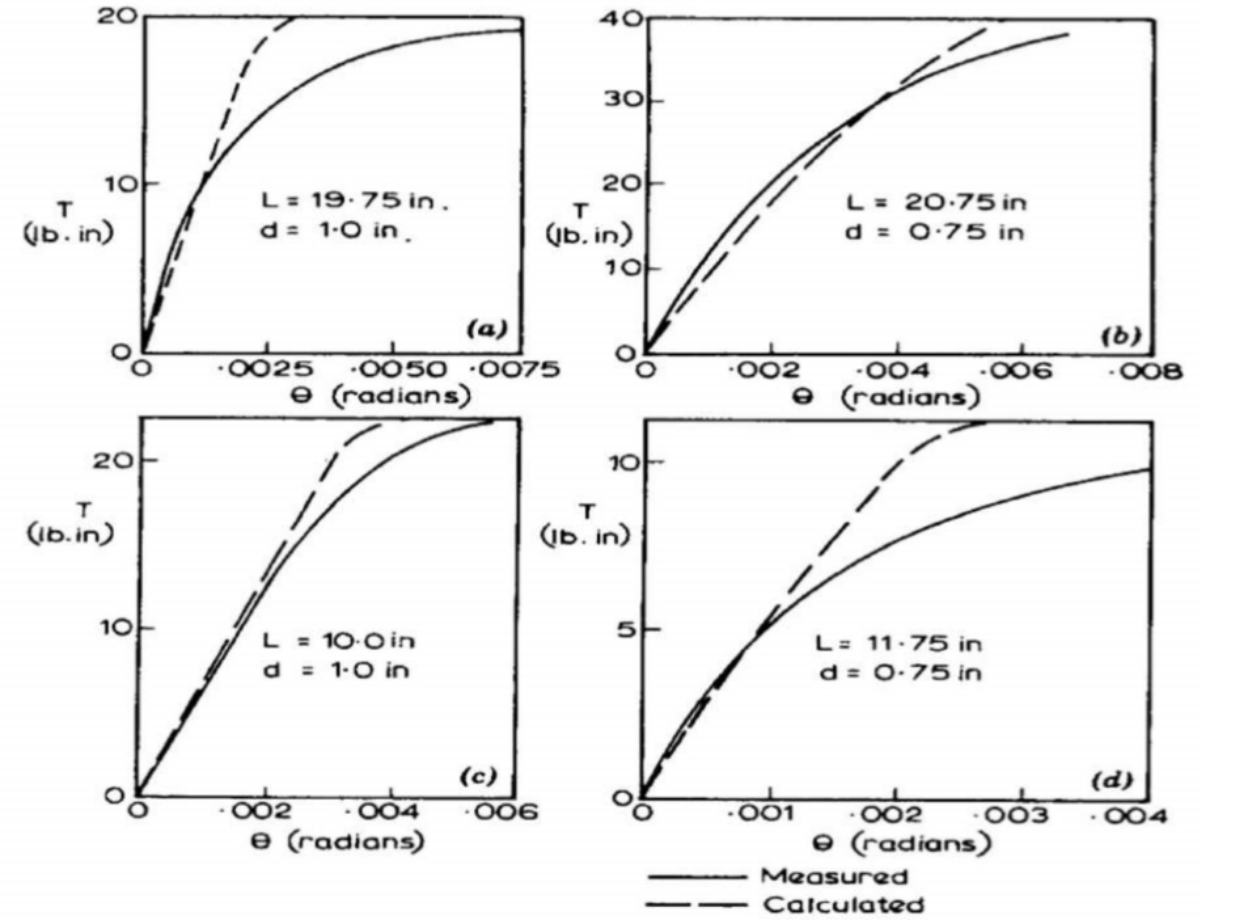

Figure 2.1. Torque versus rotation for unfinned piles in kaolin clay (Poulos 1975).

Torsional capacity of piles in sand was first studied by Dutt (1976) and Dutt and O'Neill (1983). The aim of their studies was to understand the effect of density and pile installation mechanism on the torsional capacity of circular and square piles. Laboratory tests were carried out on two circular aluminum piles with 48 mm (1.9 in.) external diameter and 2.5 mm (0.1 in.) wall thickness and two square piles with 51 mm (2.0 in.) outside dimensions and 3.2 mm (0.125 in.) wall thickness. The test box used in the study had a diameter of 1.524 m and the test configuration is shown in Figure 2.2. In situ pile installation was carried out by placing the pile in position and pluviating sand to required density around the pile, while driven tests were carried out by driving certain lengths of pile into the sand using different driving mechanisms. The piles were tested at high relative density (~80%) and low relative density (40%). Figure 2.3 shows the relationship between applied torque and pile head twist. The results showed that pile head torque resistance increases with an increase in sand density. The pile driving also influenced torsional capacity, as the driven piles had slightly higher torsional resistance than the in-situ piles. The study also noted that an increase in embedment length resulted in an increase in torsional resistance.

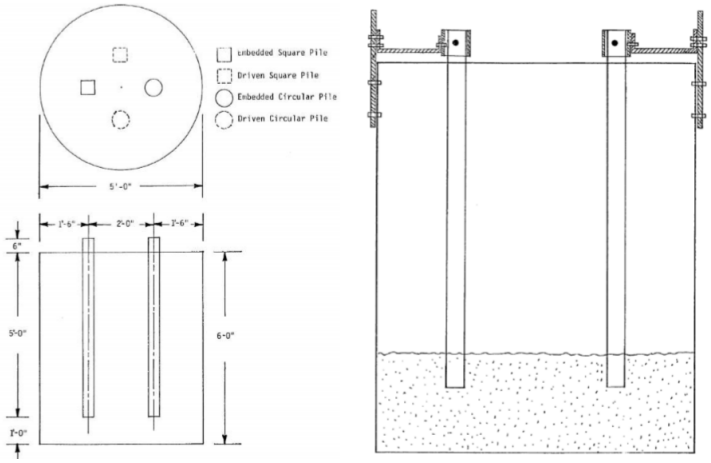

Figure 2.2. Test assembly for torsional studies in sand (Dutt 1976).

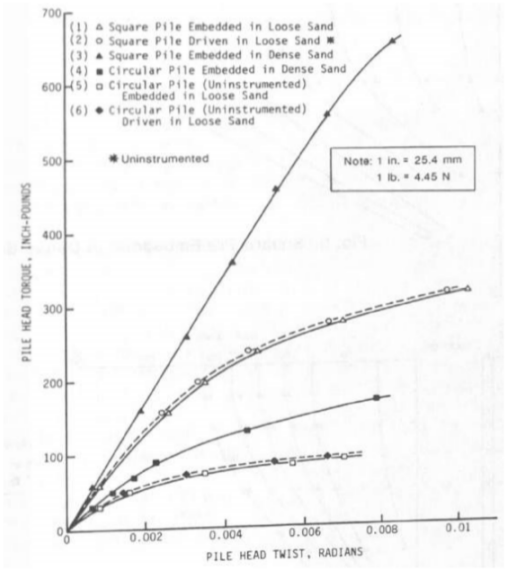

Figure 2.3. Torque versus pile head twist for unfinned piles in sand with different installation method and pile geometry.

Tawfiq (2000) used a 1.2-m (4-ft) diameter and 1.5-m (5-ft) deep steel chamber (Figure 2.4) to carry out torsional tests on a small-scale pile model in sand to understand the toe and side frictional resistance provided against torsional load. The concrete pile used for the study had a length of 508 mm (20 in.) and a diameter of 102 mm (4 in.). Torque was applied using a loading wheel and two 20-gallon buckets, filled with water at a constant flow rate, to achieve a constant loading rate. The toe and side frictional resistance for the considered section is shown in Figure 2.5. Tests by Tawfiq (2000) indicated that the side frictional resistance constituted about 91 percent of the total torsional resistance.

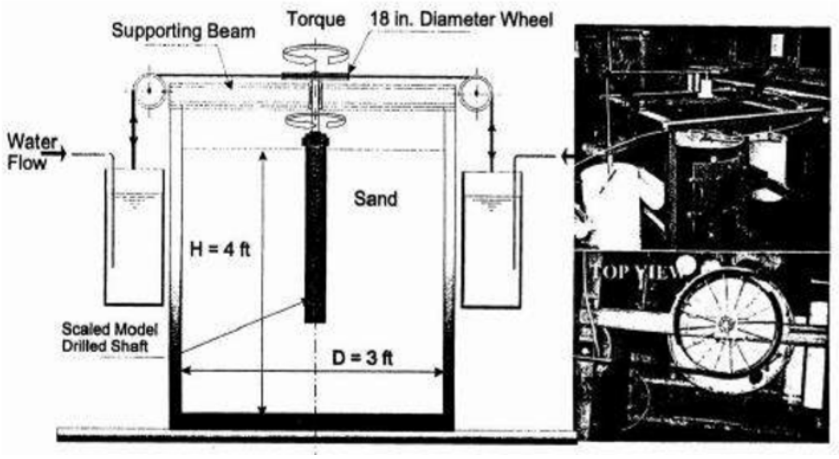

Figure 2.4. Torsional test assembly for torsional studies in sand (Tawfiq 2000).

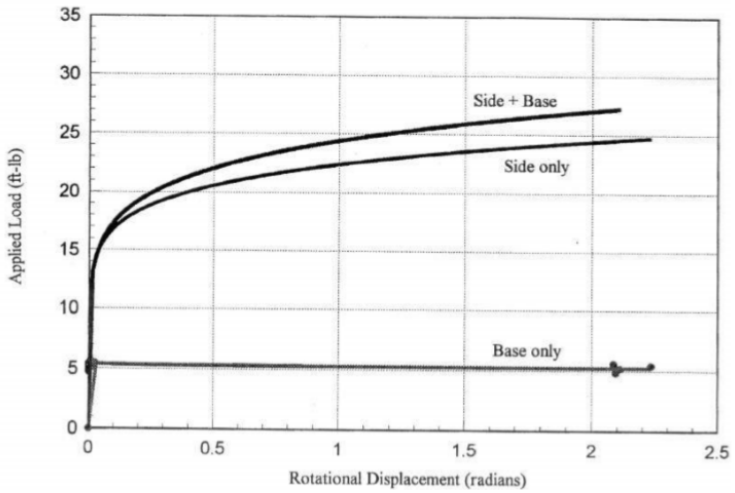

Figure 2.5. Relationship between torque and rotational displacement (Tawfiq 2000) to understand the side and base resistance of unfinned pile.

2.2.2 Centrifuge Tests on Piles

Bizaliele (1992) conducted static tests on aluminum model piles with 21-mm (0.83-in.) diameter, 1-mm (0.04-in.) wall thickness, and 340-mm (13.4-in.) embedded length in sands. The model was tested at an acceleration level of 50 g, simulating a prototype pile of 1.05-m (41-in.) diameter and 17.0-m (56-ft) embedded length. Applied torque and angular rotation were measured using a load cell and linear variable displacement transducer (LVDT), respectively. The sand used in the test was uniformly graded with an effective grain size D_{10} of 0.12 mm, an internal friction angle of 38°, and maximum and minimum dry densities of 1.69 and 1.42 g/cm^3, respectively. Figure 2.6 shows the centrifuge model setup. Static pile head torque-twist behavior is depicted in Figure 2.7. A linear response was observed for applied torque up to 8N-m (6 lb-ft); the response transitioned to nonlinear for larger torsion. The maximum torque was

approximately 28N-m (24 lb-ft) at approximately 0.07 radians of pile head twist, followed by a softening behavior.

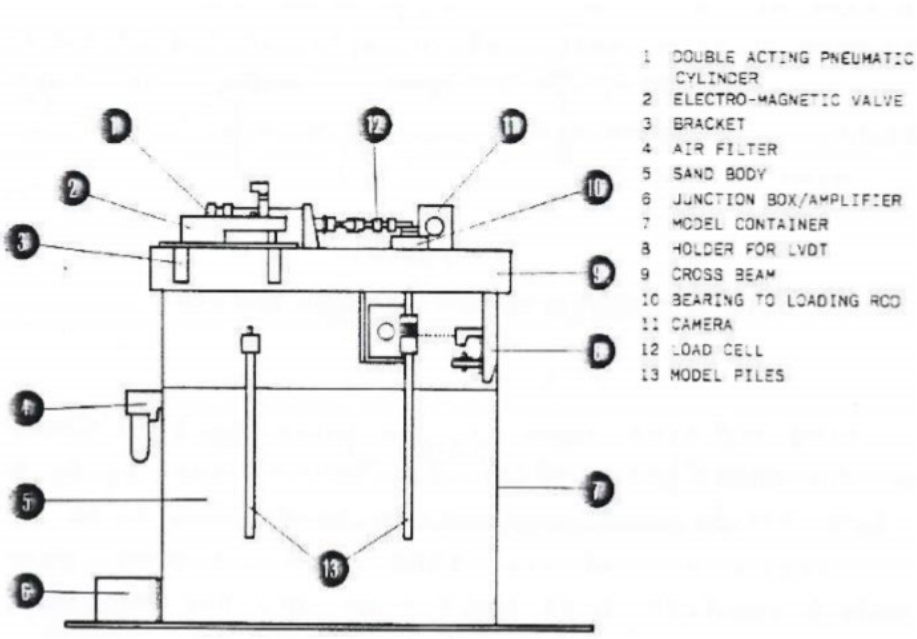

Figure 2.6. Centrifuge model setup (Bizaliele 1992).

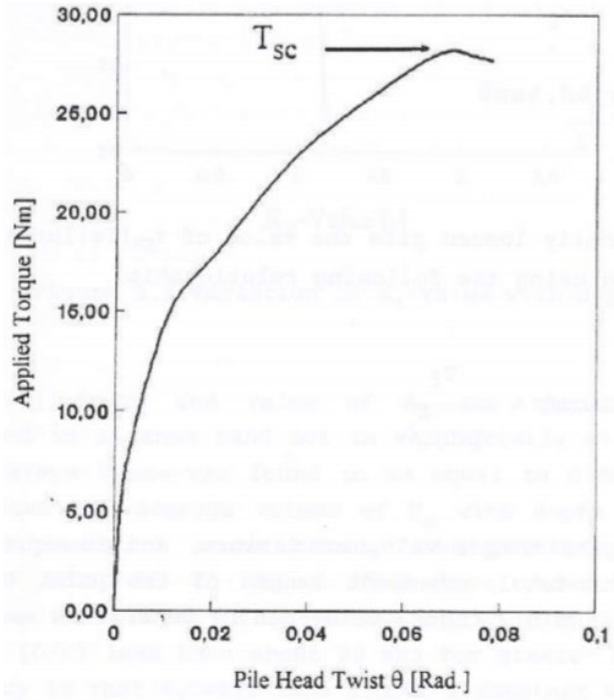

Figure 2.7. Relationship between torque and rotational displacement (Bizaliele 1992).

Laue and Sonntag (1998) performed centrifuge tests on a hollow aluminum model pile with a diameter of 15 mm (0.6 in.) and a length of 170 mm (6.7 in.) in sand to understand the effect of interface roughness on the maximum pile-head torque resistance. The model was accelerated to an acceleration of 100 g with prototype having dimensions of 1.5-m (5-ft) diameter and 17.0-m (56-ft) length. The tests were carried out in dense sand on two sand types: (a) Norm sand (angle of internal friction = 38°) and fine Fontainebleau sand (angle of internal friction = 37°). For the tests considered, different nomenclature is used for the piles. TP 2.1 and TP 3.2 represent piles with smooth and rough interface, respectively, tested in norm sand; TP 6.1 and TP 6.2 represent smooth pile and rough pile, respectively, tested in Fontainebleau sand. Figure 2.8 shows the torque-rotation response under different soil-pile interface and soil tested. The torque-angle of rotation response of smooth-piles was consistent with a hyperbolic relationship, while the rough-piles exhibited a near-linear perfectly plastic response. It is noted from Figure 2.8 that the peak torque obtained was highest for the rough-interface piles, while smooth-interface piles showed a softer response.

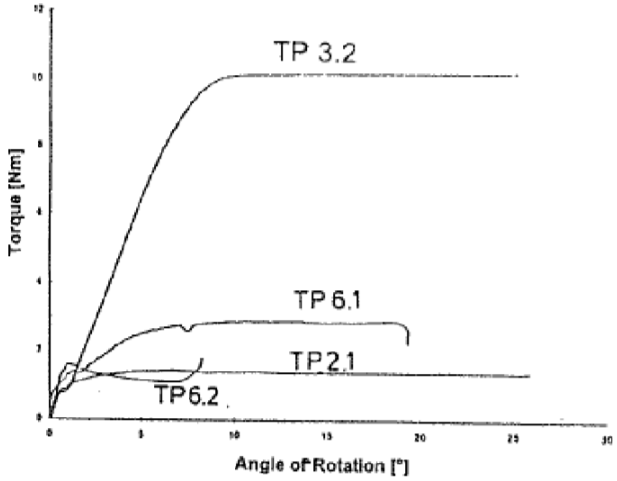

Figure 2.8. Relationship between torque and rotational displacement (Laue and Sonntag 1998).

Zhang and Kong (2006) studied torsional load transfer in model aluminum tubes of 300-mm (1-ft) length, 15.7-mm (0.6-in.) outside diameter, and 0.9-mm (0.035-in.) wall thickness. The model tubes were subjected to 40-g acceleration. The corresponding prototype length, outside diameter, and wall thickness were 12 m (39 ft), 628 mm (24 in.), and 36 mm (1.4 in.), respectively. Quartz-based uniform sand with D_{50} of 0.14 mm was used. Tests were carried out to understand the effect of sand density on torsional capacity of piles. Tests were also carried out at different loading rates to study the effect of loading rate on the torsional capacity of unfinned piles. Specimens were prepared at relative densities of 32% and 75%. Figure 2.9 shows the layout of the centrifuge tests carried out and Figures 2.10(a) and 2.10(b) show the torque versus angle of twist for different densities. With a rotation of 1°, the applied torque was about 75% and 57% of the torsional capacity in the loose sand and dense sand, respectively. The torsional resistance was almost fully mobilized at approximately 4° for all of the cases. As expected, the relative density of the sand had a significant influence on the torsional resistance. Zhang and Kong (2006) noted that the strain rates did not significantly affect the torsional resistance of the pile, as shown in Figure 2.11.

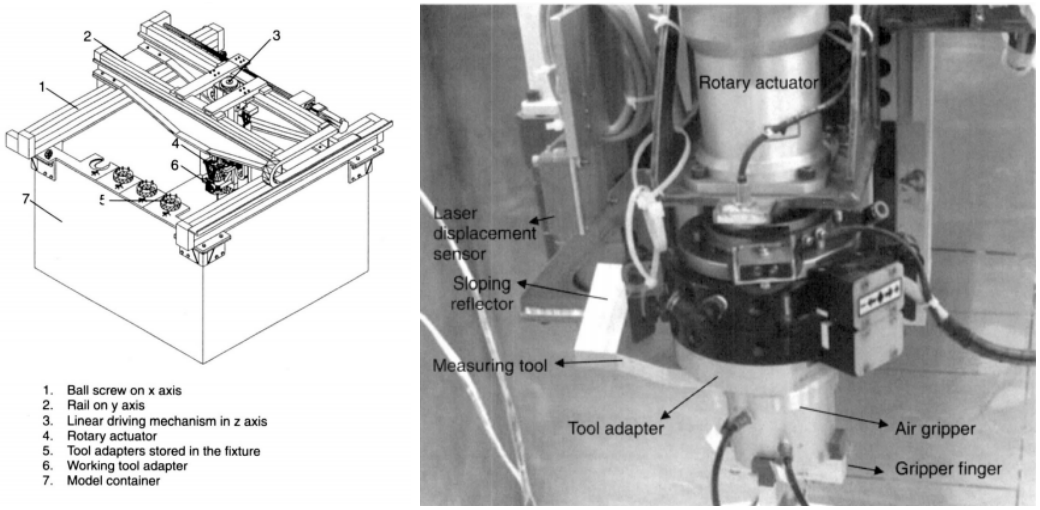

Figure 2.9. Centrifuge test assembly showing detailed test setup and loading arm for torsional testing in sand (Zhang and Kong 2006).

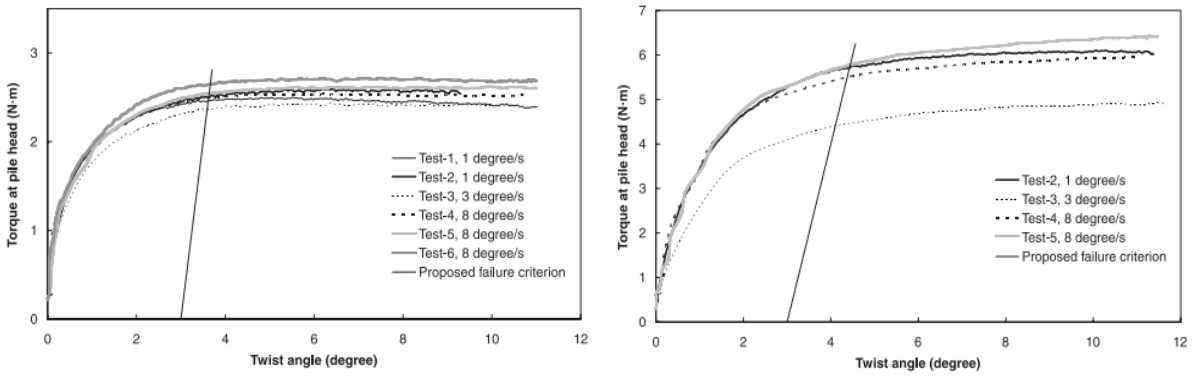

Figure 2.10. Relationship between torque and rotational displacement along with the failure criteria: (a) loose sand; (b) dense sand (Zhang and Kong 2006).

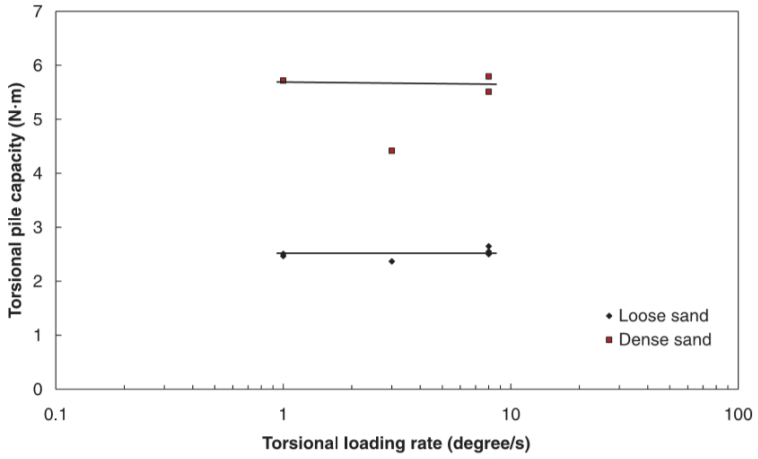

Figure 2.11. Effect of loading rate on torsional pile capacity (Zhang and Kong 2006).

2.2.3 Field Studies on Piles

Stoll (1972) carried out torsional studies on in-situ piles by applying torque on two driven steel pipe piles filled with concrete. The steel pipe piles were of 0.27-m (10.75-in.) external diameter and 6.3-mm (0.25-in.) wall thickness. Figure 2.12 shows the test setup in the field and Figure 2.13 shows the soil profile obtained from the field boring logs. Soil around the pile was heterogeneous with a final penetration resistance of 50 to 60 blows/ft. The embedded pile lengths were 17.4 m (57 ft) and 20.7 m (68 ft). Torque and rotation on top of each test pile were monitored and are shown in Figure 2.14. The torsional resistance of both piles increased with an increase in pile rotation until failure at approximately 0.055 radians (3.2°). The tests did not show any peak.

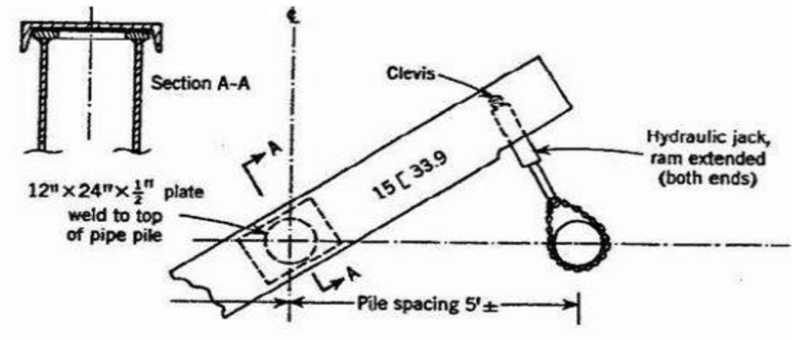

Figure 2.12. Field test setup (Stoll 1972).

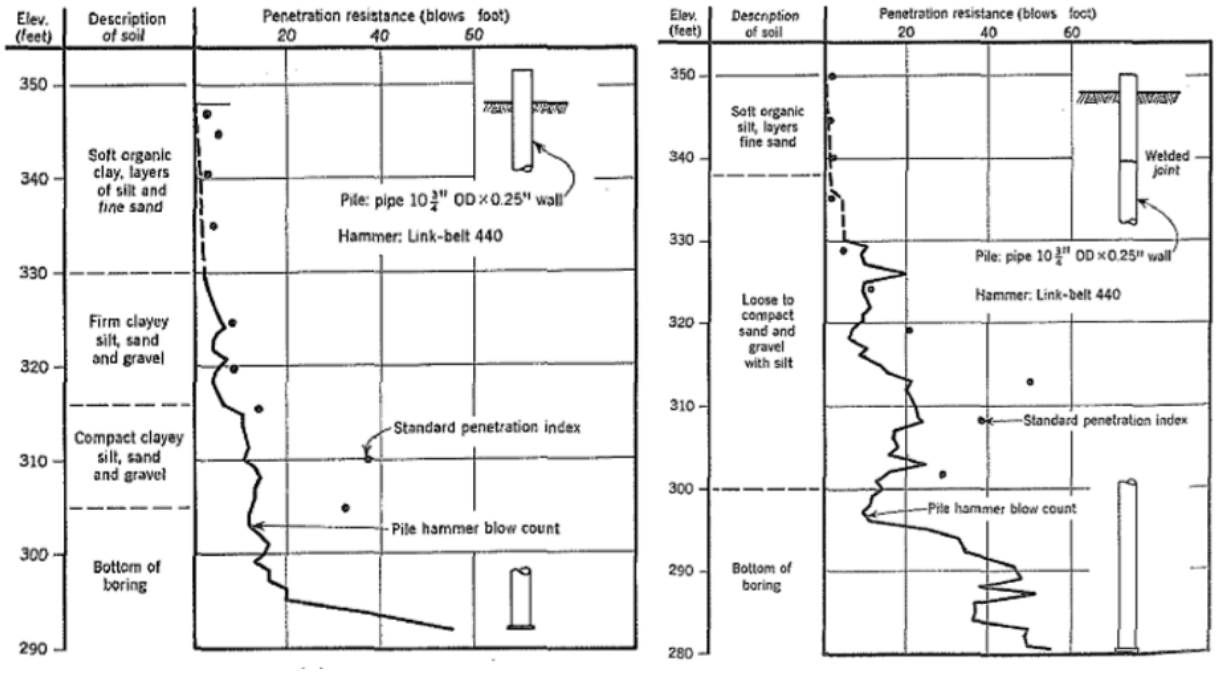

Figure 2.13. Soil profile at the site for piles: (a) pile A-3; (b) pile V-4 (Stoll 1972).

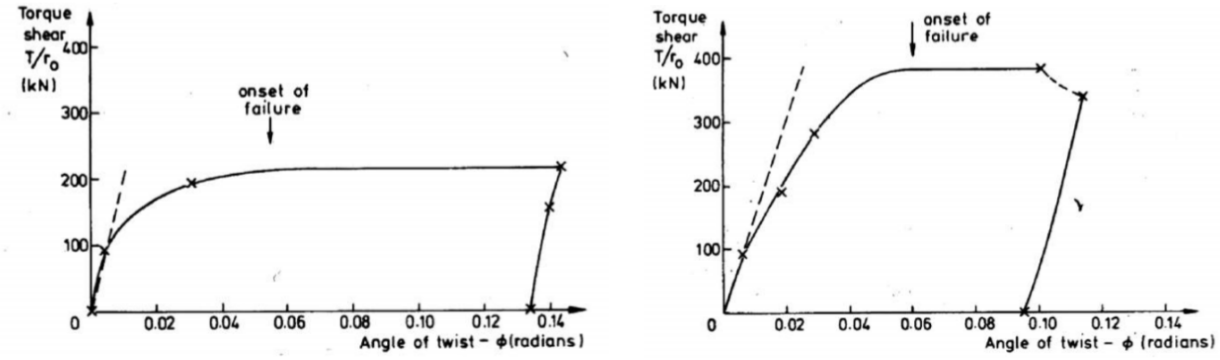

Figure 2.14. Relationship between torque and rotational displacement for: (a) pile A-3; (b) pile V-4 (Stoll 1972).

Li et al. (2017) noted that the understanding of the actual resistance to torsion provided by drilled shafts and deep foundation elements is not well established. Therefore, Li et al. (2017) and Stuedlein et al. (2016) carried out field experiments on well-instrumented drilled shafts to evaluate the torsional capacity and load transfer at full scale. One drilled shaft was constructed using typical production methods (designated TDS), whereas the other was constructed with a relatively frictionless base (designated TDSFB) to facilitate observation of possible differences in base resistance between the otherwise identical shafts. The test setup layout used in the study is shown in Figure 2.15 and the subsurface profile of the test area is shown in

Figure 2.16. Results of the torque versus angular rotation are shown in Figures 2.17(a) and 2.17(b). Hyperbolic models were used to extrapolate τ-θ curves for shaft TDS. Shaft TDSFB was constructed within one relatively uniform layer of overconsolidated clayey silt; however, TDS penetrated a layer of silty sand, and the difference in subsurface conditions yielded significant differences in the observed performance. At the end of monotonic, quasi-static loading, TDSFB had rotated approximately 13°, whereas TDS only rotated 0.14°.

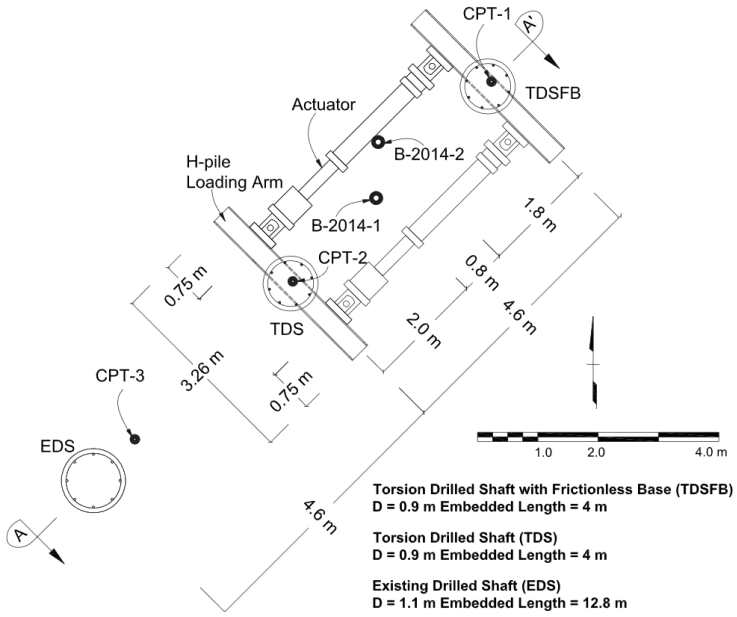

Figure 2.15. Test site layout, including the torsion drilled shaft with frictionless base, torsion drilled shaft, and existing drilled shaft (EDS), and exploration plan (Stuedlein et al. 2016).

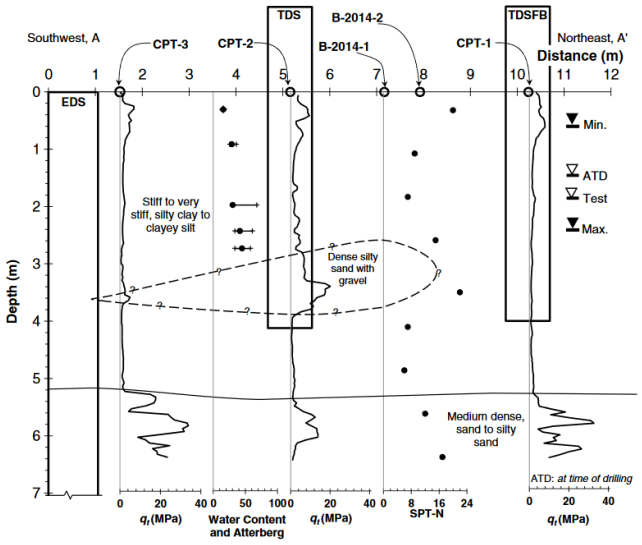

Figure 2.16. Subsurface profile at test site indicating the location of the test shafts (Stuedlein et al. 2016).

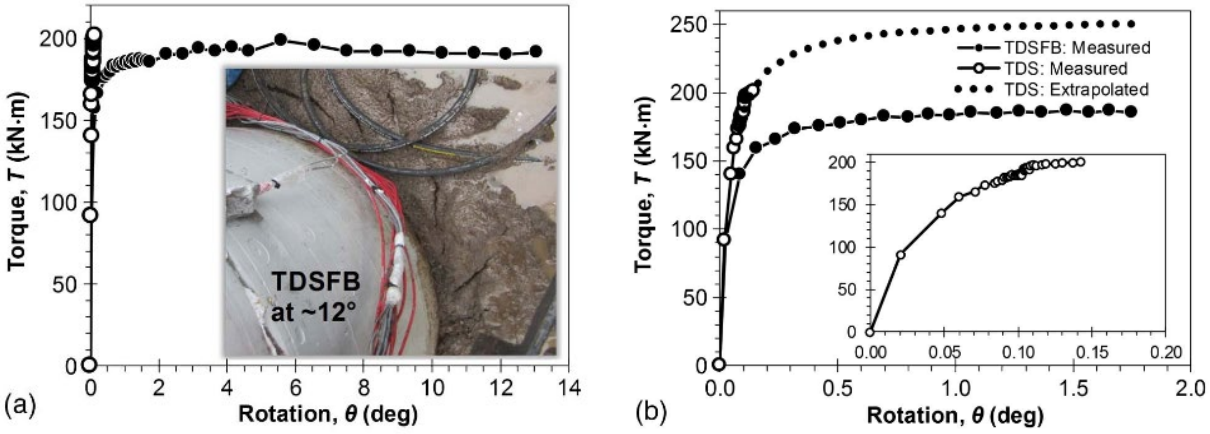

Figure 2.17. Relationship between torque and applied rotation for the test shafts under quasi-static loading: (a) full results to very large rotations of TDSFB with inset photo showing ground cracking; (b) observed and extrapolated torque and applied rotations, with inset showing the small rotation response of TDS (Stuedlein et al. 2016).

2.3 FAILURE CRITERIA FOR PILES SUBJECTED TO TORSION

For shafts subjected to torsional loading, two different criteria can be used to determine the failure of piles. According to the criteria used by Dutt and O'Neill (1983) and Randolph (1983), failure occurs when the rate of shear stress increase with rotation is zero. According to the second criterion, a critical twist angle is used to define "failure," and the torsional capacity is taken to be the torque at the critical twist angle (Zhang

and Kong 2006). However, a constant critical twist angle might not provide the maximum torsional stress mobilization; therefore, a new failure angle θ is proposed and is given by

$$\theta = \frac{180\,T\,L_p}{\pi\,G\,I_p} + C \tag{2.1}$$

where T is the applied torque at the pile head; L_p is the pile length; G is the shear modulus of the pile; I_p is the polar moment of inertia of the pile; and C is the toe twist angle at failure. Variation of this proposed θ for the test results is shown in Figure 2.10.

2.4 STUDIES ON LATERAL LOAD CAPACITY OF SFPFs

2.4.1 Laboratory and Numerical Studies on SFPFs and Unfinned Piles

Duhrkop and Grabe (2008) carried out laboratory experiments on piles with fins to understand the effect of fin shape on lateral load response. For the tests, a plastic tube with a diameter of 110 mm and a length of 450 mm was used with fins of different shapes as shown in Figure 2.18. Lateral load tests were carried out on these piles until a lateral displacement of 40 mm, and the lateral load (P) versus lateral displacement (δ) for these tests is shown in Figure 2.18. Test results demonstrate that all fin shapes resulted in an increase in the lateral load-bearing capacity with rectangular fins showing the best performance.

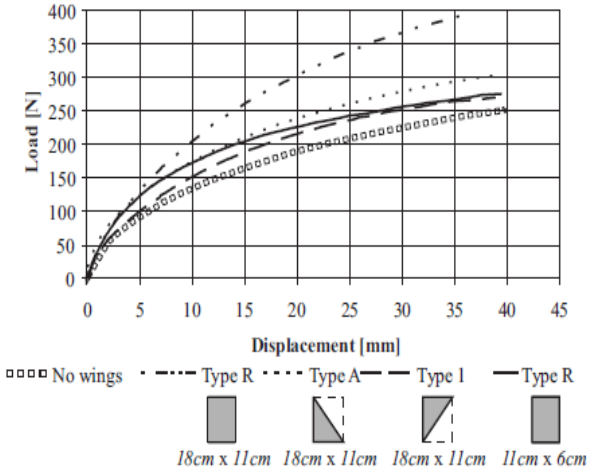

Figure 2.18. Effect of fin geometries on load versus displacement (from Duhrkop and Grabe 2008).

Nasr (2013) carried out tests using a long, flexible pile (L_P = 777 mm) in loose sand (D_r = 35%) with one test using triangular fin with the width decreasing with depth and another test with rectangular fin. Both configurations have the same maximum fin width and fin length. Figure 2.19 presents the dimensions of SFPFs used by Nasr (2013). The pile head load versus displacement from the test is presented in Figure 2.20. It can be observed that the lateral displacement at the ground surface for piles with rectangular and triangular fins decreased by 70% and 37%, respectively, from that of the unfinned pile. Hence, both the Duhrkop and Grabe (2008) and Nasr (2013) studies indicated that rectangular fins are more effective in reducing the lateral pile head deflection and increasing the ultimate lateral load of the pile.

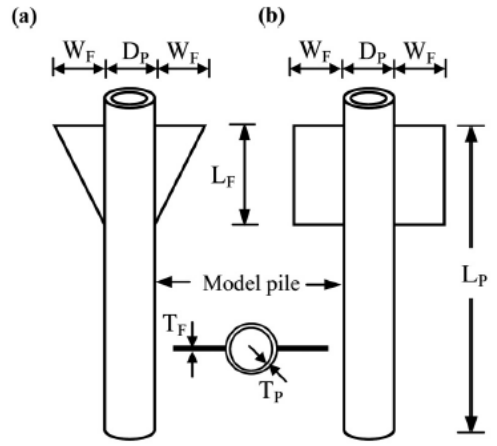

D_P = pile diameter (constant); L_P = embedded length of pile; W_F = fin width; L_F = fin length; T_P = thickness of pile wall; T_F = thickness of fin wall (constant).

Figure 2.19. Dimensions of finned piles: (a) triangular fin pile; (b) rectangular fin pile (from Nasr 2013).

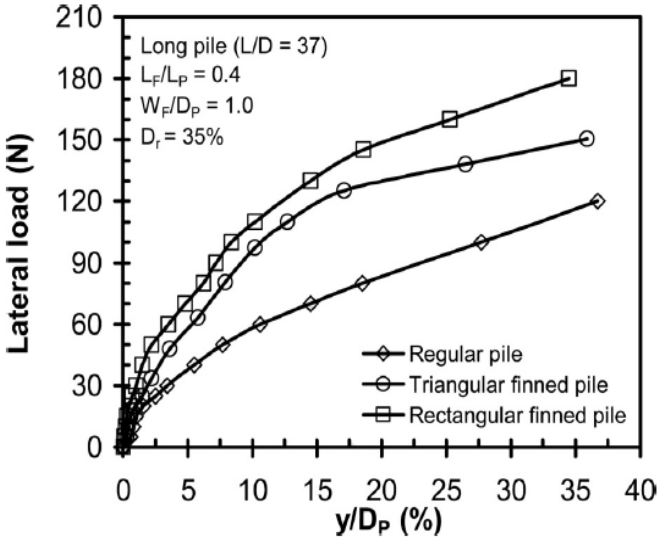

Figure 2.20. Lateral load versus deflection for regular and triangular finned piles (from Nasr 2013).

Babu and Viswanadham (2018) studied the effect of fin location on the lateral load capacity of SFPFs using the finite element package, Abaqus, in medium dense sand. In the simulation, two pairs of 100-mm-long by 20-mm-wide fins were installed at the top, middle, and bottom of a 400-mm-long by 44.5-mm-diameter pile. The pile head was loaded to a lateral displacement of 10% of the pile diameter. The results are presented in Figure 2.21. The findings of Babu and Viswanadham (2018) are in general agreement with

Peng et al. (2010) that the fin is most effective near the ground surface, and this effect decreases as the depth of fins increases.

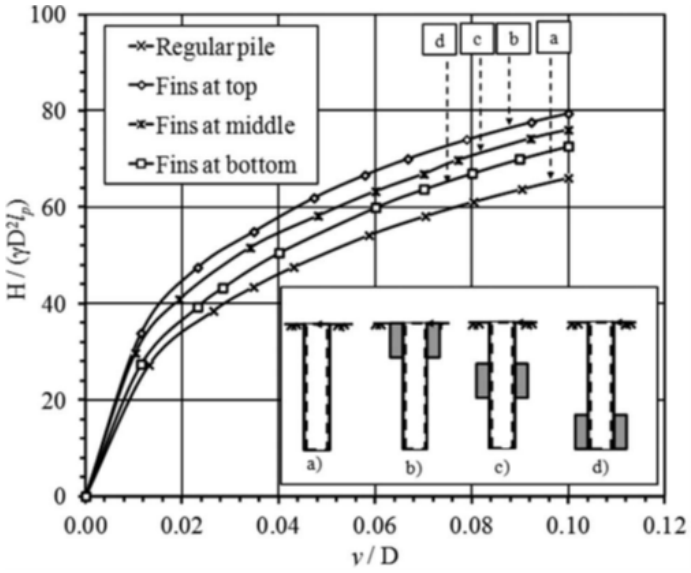

Figure 2.21. Load-displacement versus fin locations (from Babu and Viswanadham 2018).

Abongo (2019) conducted simulations to study the optimal SFPF fin width and length under lateral loading using Plaxis-3D. In the simulations, fins with different width of the fin (W_F) to pile diameter (D_P) ratios but a fixed fin length (L_F) were modeled on the same pile and tested under the same soil condition. Both pile head rotation efficiency and pile head lateral displacement efficiency versus W_F/D_P were reported. The results are presented in Figures 2.22 and 2.23. From these two figures, it can be concluded that the increase in lateral rotation efficiency and load efficiency begins to plateau when W_F/D_P exceeds 1.0. Therefore, the optimal W_F/D_P ratio is about 1.0 for SFPFs, which is in agreement with Nasr (2013).

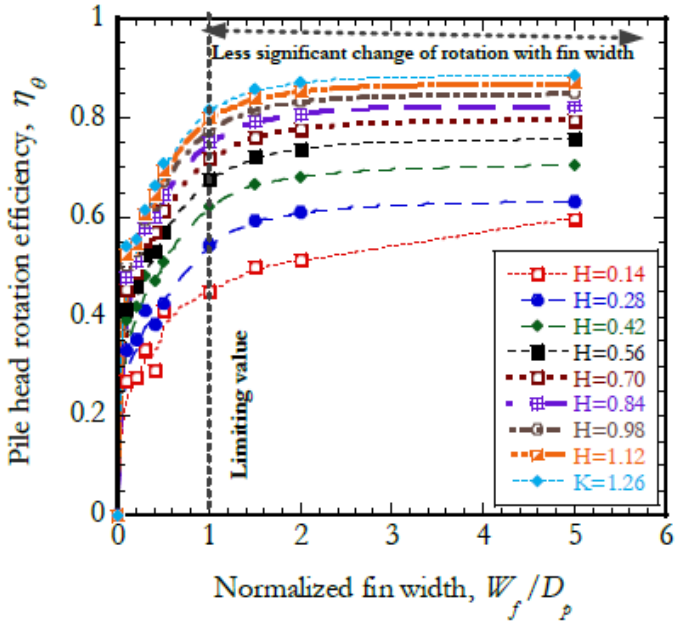

Figure 2.22. Pile head rotation efficiency versus W_F/D_P (from Abongo 2019).

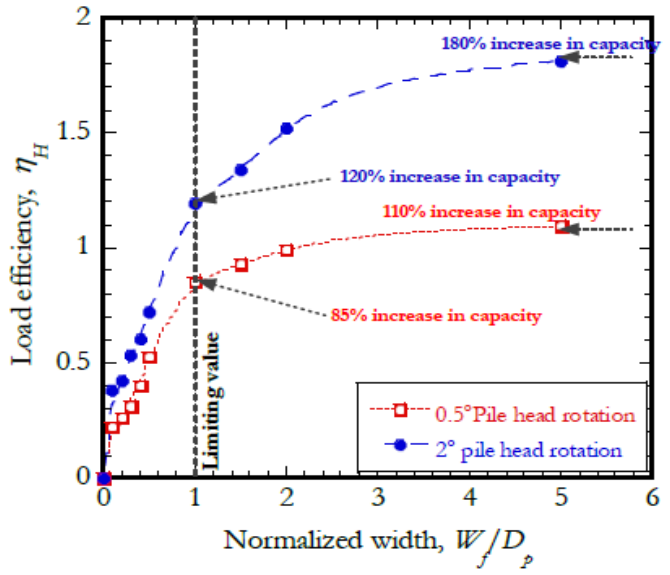

Figure 2.23. Pile head load efficiency versus W_F/D_P (from Abongo 2019).

Abongo (2019) investigated the optimal fin length for SFPFs under lateral loading numerically using Plaxis-3D. In the simulations, fins with different lengths but fixed width were modeled on the same pile as mentioned in the previous paragraph. Figure 2.24 presents pile head rotation efficiency with fin length. Similar to the findings of Nasr (2013), all SFPFs show an increase in efficiency over the unfinned pile (i.e., $L_F/L_P = 0$). However, as the L_F/L_P ratio increases beyond 0.4, the increase in pile head rotation efficiency becomes less significant.

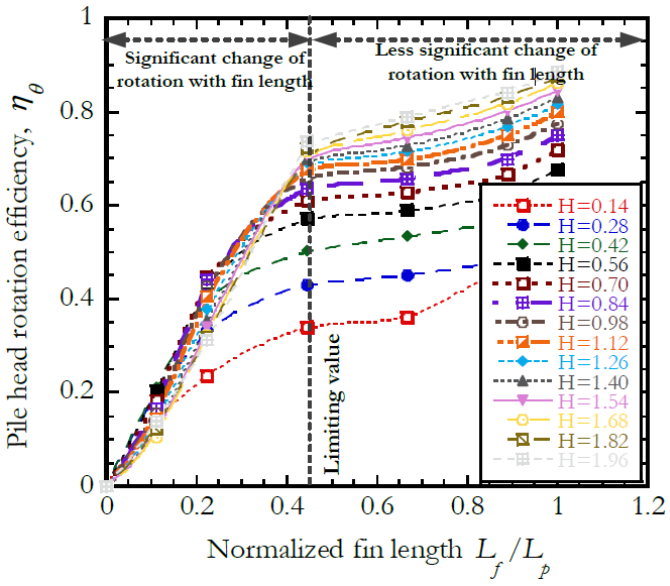

Figure 2.24. Pile head rotation efficiency versus L_F/L_P (from Abongo 2019).

2.4.2 Field Testing of SFPFs

A typical field test of SFPFs involves three stages: (1) obtaining soil profiles from site exploration such as the standard penetration test (SPT) and cone penetration test (CPT); (2) pile installation through static, dynamic, or a combination of static and dynamic forces; and (3) external load application to the pile. Instrumentation needed for field test includes load cell, displacement gauge, strain gauge, inclinometer, hydraulic jack, and loading bracket. Figure 2.25 presents a photo of the instrumentation from Murphy et al. (2016). Figure 2.26 presents the SFPF geometry and install location of strain gauges from Murphy et al. (2016).

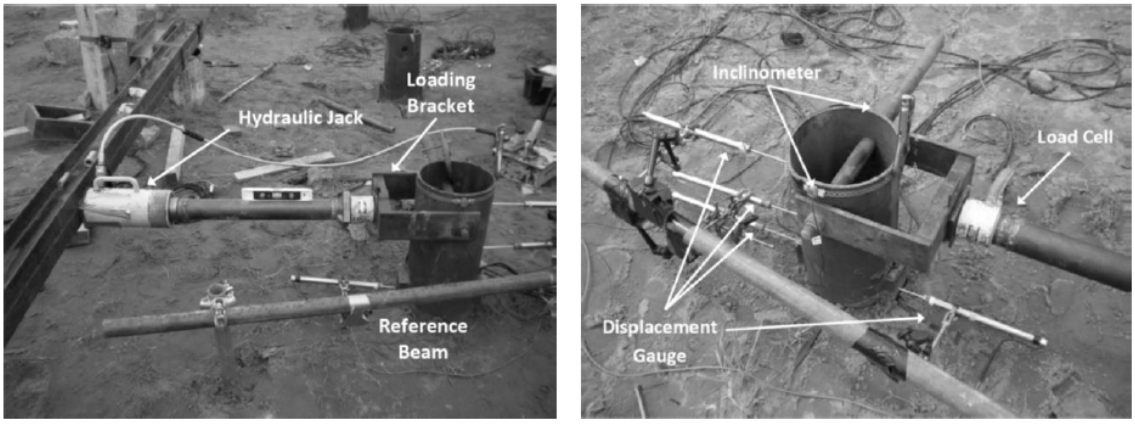

Figure 2.25. Photos of test instrumentations (from Murphy et al. 2016).

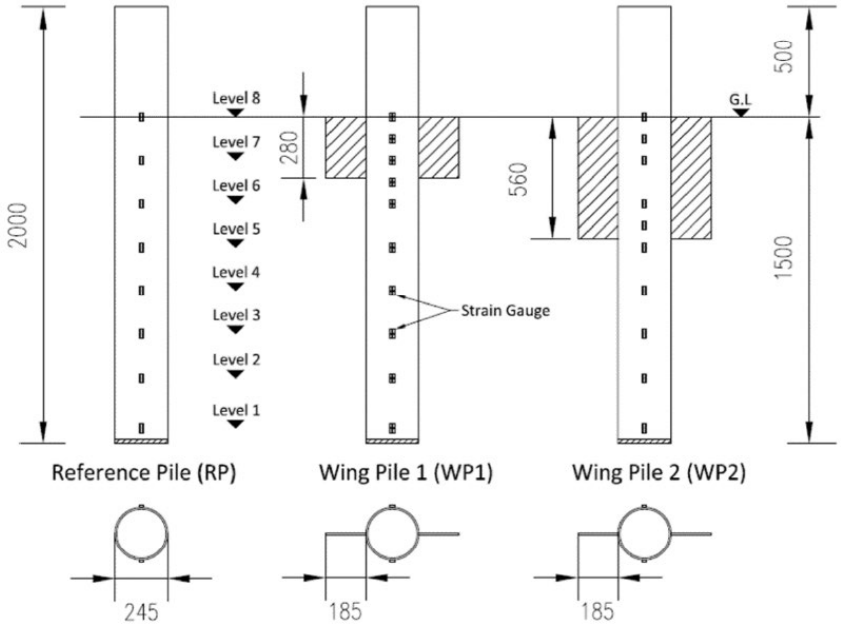

Figure 2.26. SFPF geometry and strain gauge configuration (from Murphy et al. 2016).

2.4.2.1 Fin Effect on SFPF Lateral Resistance Capacity

Murphy et al. (2016) conducted field tests at two sites to study the lateral load-carrying capacity of SFPFs in comparison to unfinned piles. Tested SFPFs and unfinned pile geometries are presented in Figure 2.26. For the two test sites, the soil was classified as dense silty sand for the Blessington site and medium dense silty sand for the Garryhesta site. Figure 2.27 presents the measured lateral load resistance versus lateral displacement at the pile head for both sites. Results demonstrate that the addition of fins improved the lateral bearing capacity and stiffness of the pile response significantly. The ultimate lateral bearing capacity increased by approximately 16% for WP1 and 36% for WP2 relative to the reference pile (RP) in the Blessington tests. For the Gerryhesta site, the ultimate lateral bearing capacity increased by approximately 17% for WP1 and 28% for WP2 relative to the reference pile. Results from these field tests are in general agreement with results derived from previously discussed laboratory tests and numerical simulations.

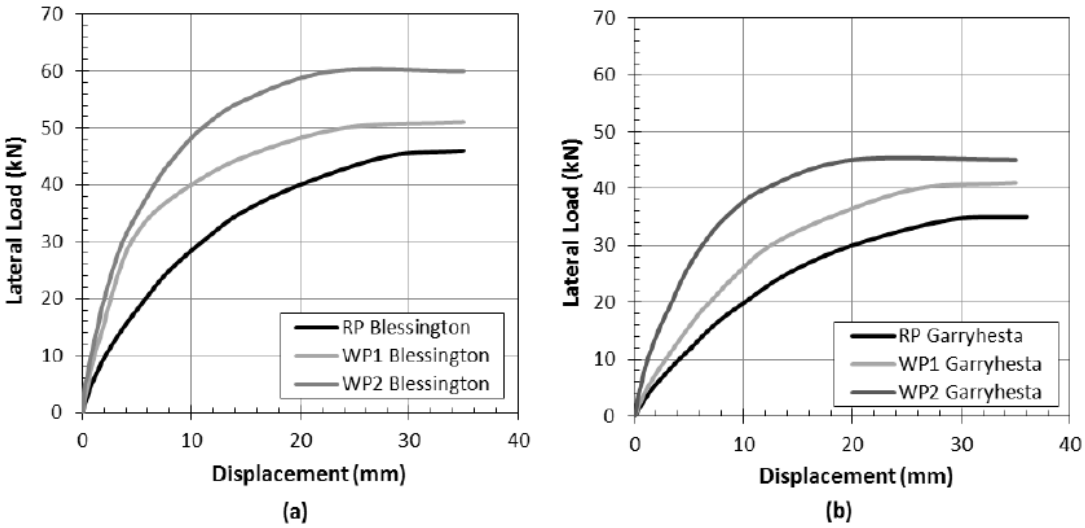

Figure 2.27. Lateral load versus displacement at: (a) Blessington site; (b) Garryhesta site (from Murphy et al. 2016).

2.4.2.2 Fin Length Effect on SFPF Lateral Resistance Capacity

Murphy et al. (2016) proposed that the efficiency of fins may be represented by comparing the ratio of the secant stiffness (k), which is the ratio of applied load to ground line displacement of SFPFs to that of the reference piles (i.e., unfinned pile). Figure 2.28 presents the results of the SFPFs secant stiffness normalized by the stiffness of the reference pile (RP). The response was broadly similar at both sites. At normalized displacements of concern for serviceability analysis ($y/D < 1.2\%$), the SFPF stiffness response with longer fins (WP2) was 2.2 to 2.7 times higher than the stiffness mobilized by the unfinned pile. This benefit is not as significant for the SFPF with shorter fins (WP1), the stiffness of which was 1.35 to 1.8 times higher than the unfinned pile over the same displacement range. For both SFPFs, the fin efficiency decreased with increasing normalized displacement level. However, even at displacement levels associated with ultimate failure (i.e., $y/D = 10\%$), the SFPFs secant stiffness was between 20% (WP1) and 40% (WP2) higher than the unfinned pile.

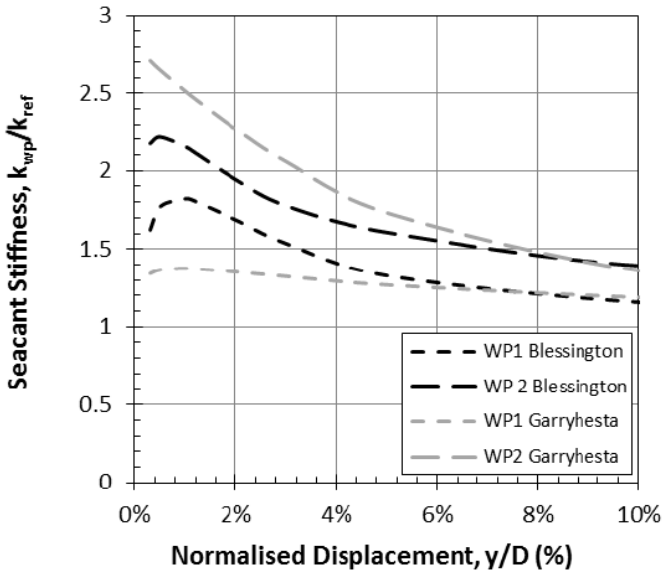

Figure 2.28. Secant stiffness versus normalized displacement (from Murphy et al. 2016).

2.4.2.3 Fin Effect on SFPF Load Transfer Mechanism

Murphy et al. (2016) reported an analysis of the bending moment distribution in the SFPFs and unfinned pile based on measured strain gauge data. Figure 2.29 presents the bending moment distribution of both SFPFs and unfinned pile. Figure 2.30 presents the displacement-depth profile of both SFPFs and unfinned pile. The bending moment was calculated using the curvature of the unfinned pile, which was obtained based on the measured compression and tension strains. Calculated total moments decrease 10-20% on average along the unfinned pile and 10%~13% in maximum bending moments in WP1 and WP2, respectively, at the same applied load, which illustrates that the maximum bending moments in SFPFs decrease with an increase in fin size. In addition, it is observed that the addition of the fins moved the point of the maximum bending moment up along the pile, which suggests that the point of rotation moved toward the ground surface. These conclusions are in general agreement with the findings reported by Nasr (2013) and Babu and Viswanadham (2018).

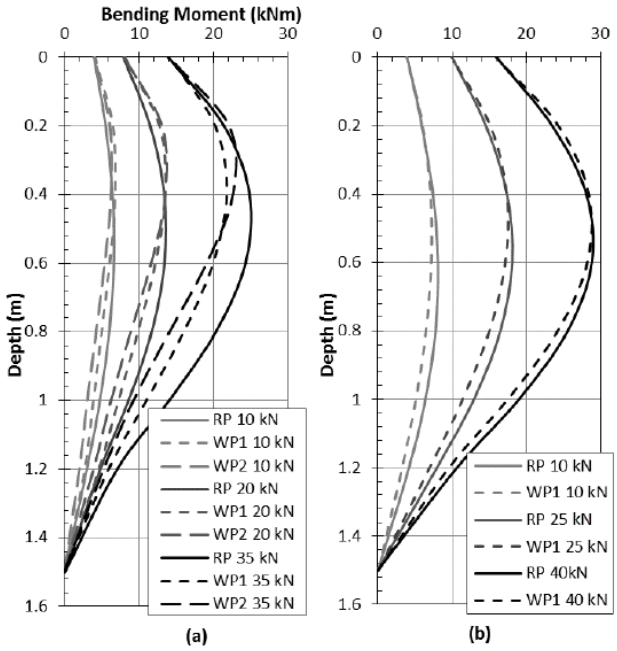

Figure 2.29. Depth versus moment in pile tests: (a) Garryhesta site; (b) Blessington site (from Murphy et al. 2016).

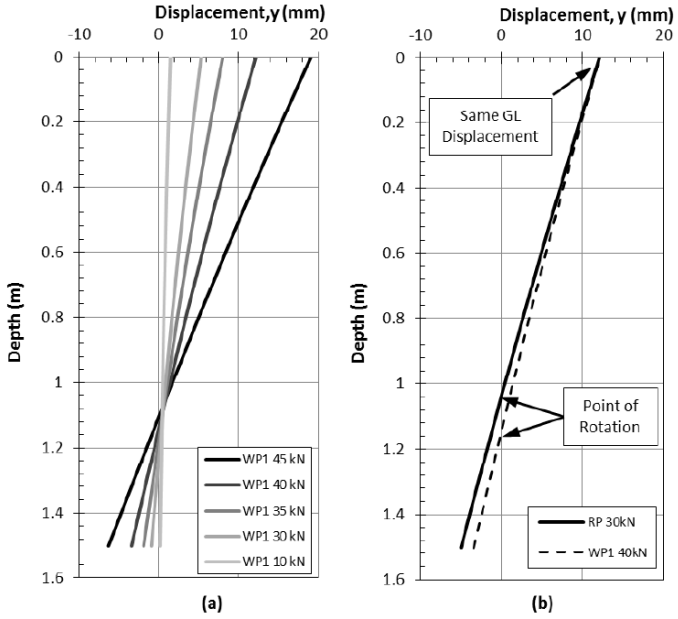

Figure 2.30. Depth versus displacement in pile tests: (a) Garryhesta site; (b) Blessington site (from Murphy et al. 2016).

Murphy et al. (2016) also reported the effect of fins on the development of soil resistance during lateral loading. Figure 2.31 presents the soil resistance along the unfinned pile at the service limit state (SLS). By comparing the increased soil resistance *(*ΔP) mobilized along the unfinned pile of each pile at fixed pile displacements (i.e., SLS displacement limit, $y/D = 1.2\%$) it was observed that the increase in soil resistance was highest over the finned portion of the pile and decreased with depth. Figure 2.32 presents the *p-y* curves at 0.2 m and 0.6 m for the unfinned pile and SFPFs. By examining the *p-y* curves below the location of the fins (i.e., at 0.6 m), the *p-y* curves in the SFPFs exhibited a stiffer soil response than that of the reference pile, suggesting that the addition of fins appeared to affect the overall stiffness response of the pile rather than just in the area of the pile where the fins were present.

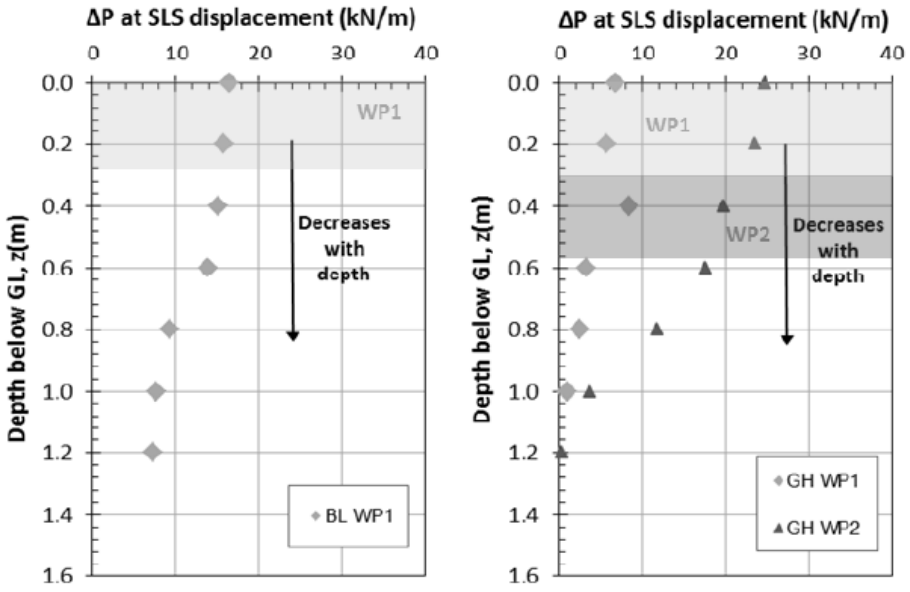

Figure 2.31. Depth versus ΔP at SLS displacement limit (from Murphy et al. 2016).

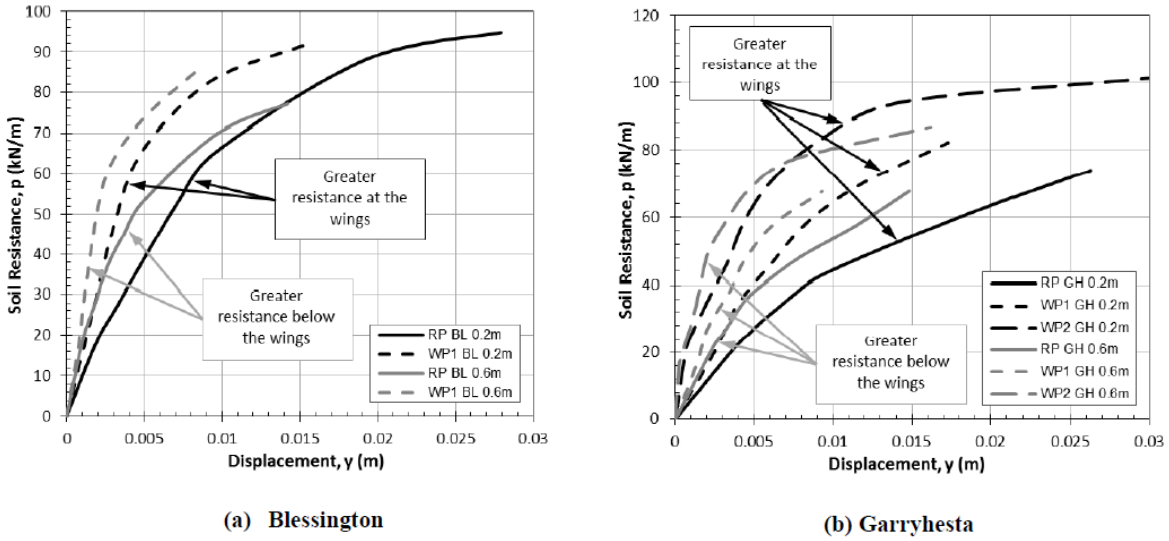

Figure 2.32. The p-y curves at 0.2 m and 0.6 m for unfinned pile and SFPFs (from Murphy et al. 2016).

2.5 FAILURE CRITERIA FOR LATERALLY LOADED PILES

Studies have used different criteria to determine the failure of laterally loaded piles and these criteria are dependent on the structure type (Meyerhof et al. 1981; GAI Consultants 1982; Fleming et al. 1992; Hu et al. 2006; Lee et al. 2013). Meyerhof et al. (1981) defined the ultimate load as the load corresponding to a large increase in lateral displacement for a small increase in the applied load. Fleming et al. (1992) defined the ultimate load as the load corresponding to a deflection of 10% of pile diameter for a circular pile. Some researchers used the angle of pile head rotation to determine the ultimate lateral load capacity of the pile. GAI Consultants (1982) and Lee et al. (2013) specified the ultimate lateral capacity at pile head rotation of 2° while Hu et al. (2006) defined the ultimate lateral capacity for traffic pole structures at pile head rotation of 1.5°. Peng et al. (2011) and Sawwaf (2006) defined the lateral capacity of unfinned piles as the load corresponding to a vertical alignment by 1.5° producing a lateral displacement between 0.1 D_p to 0.2 D_p at the ground surface. Lee et al. (2010) showed that the lateral load criteria defined by Meyerhof et al. (1981) are in agreement with the ultimate load defined as per GAI Consultants (1982), as the ultimate loads obtained from both of these methods were similar.

2.6 POINT OF ROTATION OF THE PILE DURING LATERAL LOADING

Rigid or short piles tend to rotate about a point when subjected to lateral loads as observed by several researchers (Prasad and Chari 1999; Abongo 2019). Several methodologies have been adopted to obtain the point of rotation of the pile. Prasad and Chari (1999) came up with Equation 2.2 to obtain the point of rotation x using the eccentricity (e) and the embedded length (L_p) of the pile.

$$x=\left[\left(-0.567L_p+2.7e\right)+\left(5.307\,L_p^2+7.29e^2+10.5\,541\,eL_p\right)^{0.5}\right]/2.1996 \qquad 2.2$$

The experimentally observed pile rotations were in agreement with the Equation (2.2) used by Prasad and Chari (1999). The value of x calculated by Prasad and Chari (1999) was 0.72 L_p while that obtained by Rutledge (1956) was 0.68 L_p. Abongo (2019) used two LVDTs to obtain the value of x experimentally and showed that for both unfinned piles and fin pile, the point of rotation was at 0.7 L_p. Li et al. (2010) showed that for unfinned piles in dense sand, values of x are large (0.8 L_p) at small lateral displacements; however, at large lateral displacements, the value decreases to 0.7 L_p.

2.7 STUDIES OF COMBINED TORSION AND LATERAL LOADING ON PILES

Centrifuge tests were carried out by McVay et al. (2003), Hu (2003), and Hu et al. (2006) on steel unfinned piles with arm attached to the top of the unfinned pile, signifying the mast lighting, signs, and signals in traffic posts. Prototype pile diameter was 1.5 m (5 ft), and embedment length ranged from 4.6 m (15 ft) to 10.7 m (35 ft). The aim of these experiments was to understand the effect of density, moment arm (torque applied/lateral load applied), and aspect ratio of pile (L_p/D_p) of piles on the pile capacity during combined lateral and torsional loads. Tests were carried out in Florida fine sand (Edgar), classified as poorly graded (SP), at three different relative densities: loose, medium and dense conditions. Configuration of the centrifuge test setup is shown in Figure 2.33. Figure 2.34 shows the lateral load versus lateral displacement during combined lateral load and torsion on sand at different relative densities and L_p/D_p ratios. The studies noted that torsion significantly reduces the lateral capacity of unfinned piles. Irrespective of L_p/D_p ratio of the unfinned pile and sand density, the capacity of piles decreases significantly with moment arm (toque/lateral load ratio) as shown in Figure 2.35. Studies on saturated soils showed that failure limit is achieved in torsional resistance well before the same is achieved in lateral loading.

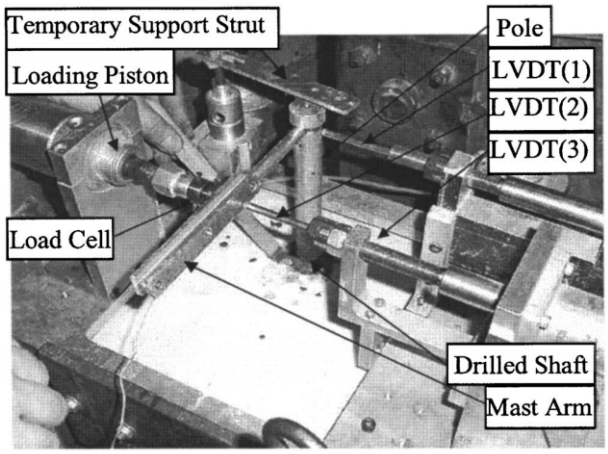

Figure 2.33. Centrifuge test assembly showing detailed test setup for torsional testing in sand (Hu et al. 2006).

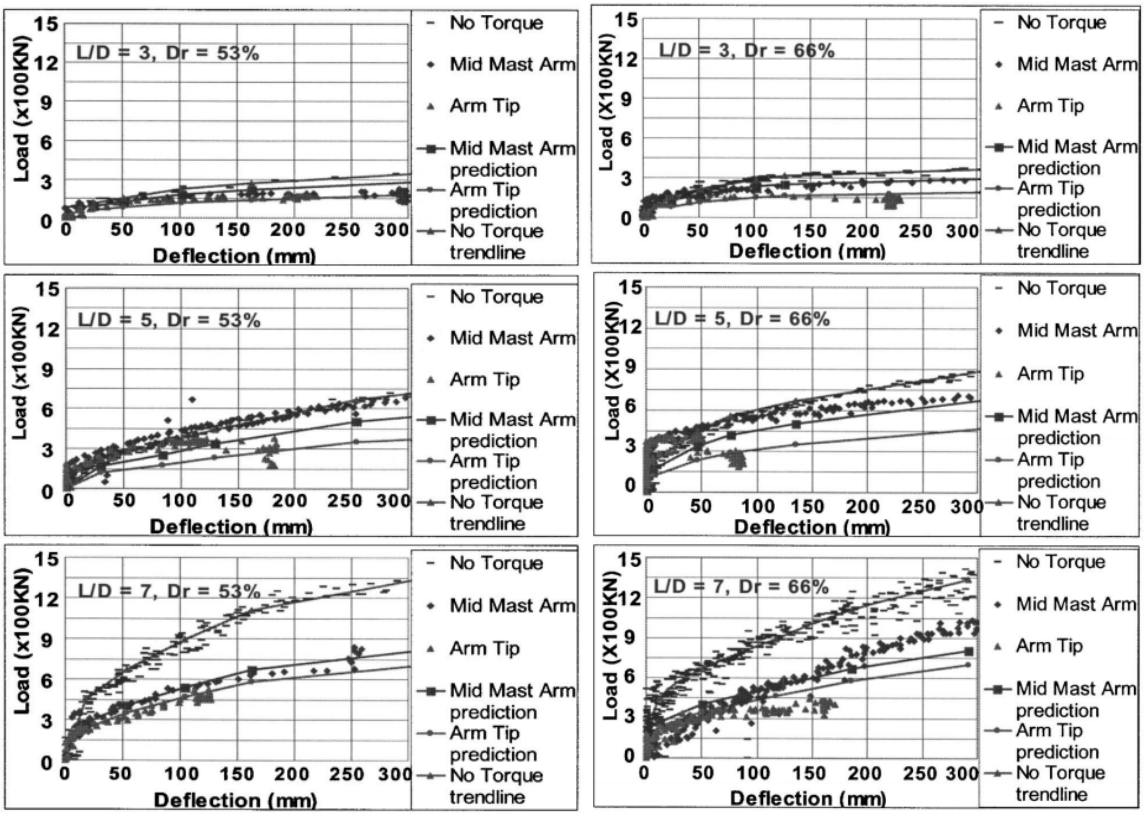

(a) (b)

Figure 2.34. Lateral load versus lateral displacement for different densities and L/D ratios of piles in sand at different densities (Hu et al. 2006).

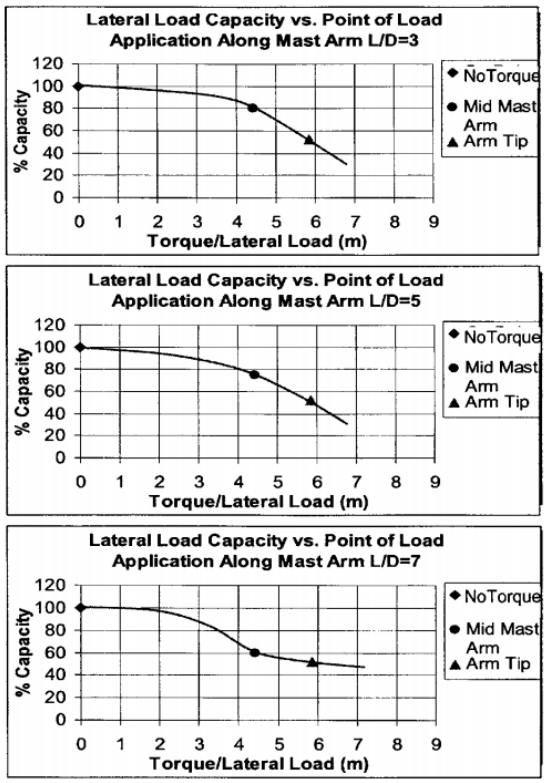

Figure 2.35. Reduction in capacity with torque/lateral load ratio for different L/D ratios considered (Hu et al. 2006).

Thiyyakkandi et al. (2016) carried out large-scale field studies using drilled shafts of different embedment lengths and fixed diameter in non-homogeneous soil to understand the effect of combined lateral and torsional load on drilled shafts. In-situ soil profile with the piles are shown in Figure 2.36. Cohesive soil is at the surface, underlain by cohesionless soil. All piles were equipped with a mast arm, which was pulled during the experiment, providing necessary lateral force and torsion. Tests were carried out on three different piles, one having a diameter of 1.22 m (4 ft) and an L_p/D_p value of 3 and the others with a diameter of 1.22 m (4 ft) and an L_p/D_p ratio of 4.5. Field test setup is shown in Figure 2.37. For long shafts ($L_p/D_p >$ 4.5), torsion mode dictated the failure mode. Figure 2.38(a) shows variation of torque with rotation for all the piles, while Figure 2.38(b) shows the lateral load versus lateral displacement for the piles. The lateral resistance is significantly reduced in the piles during the simultaneous application of torsion and lateral load, as limiting angular rotation is reached before limiting lateral displacement. Reduction in lateral resistance continues linearly with an increase in moment arm. Therefore, the study recommends that reduced lateral load resistance be used during foundation design.

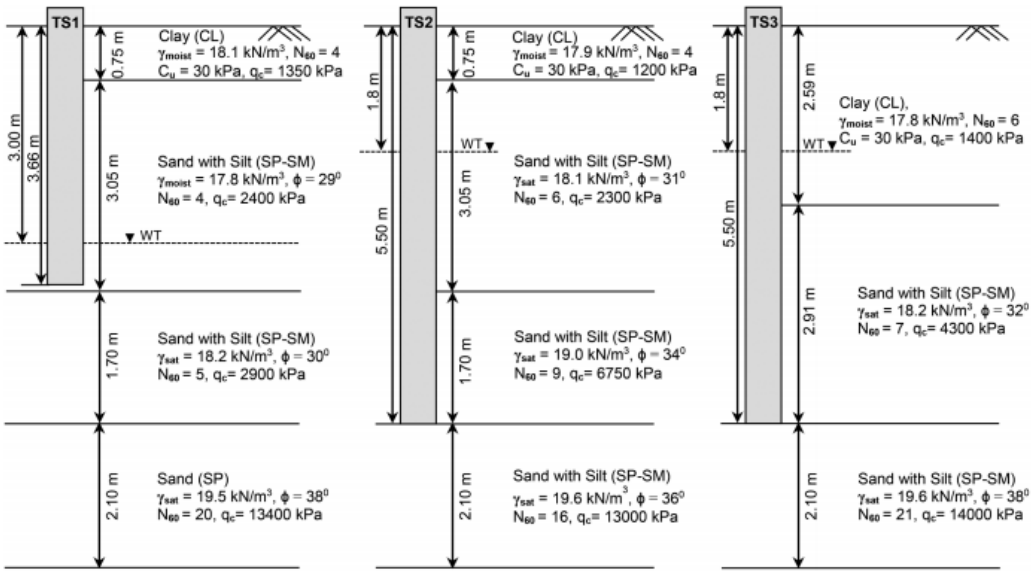

(a) (b) (c)

Figure 2.36. Soil profile for different pile depths: (a) TS-1; (b) TS-2; (c) TS-3 (Thiyyakkandi et al. 2016).

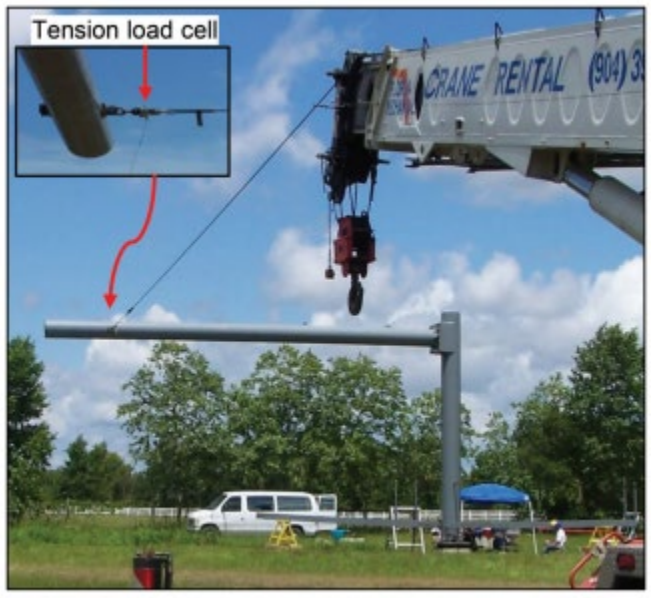

Figure 2.37. Field test setup for combined torsional and lateral load testing (Thiyyakkandi et al. 2016).

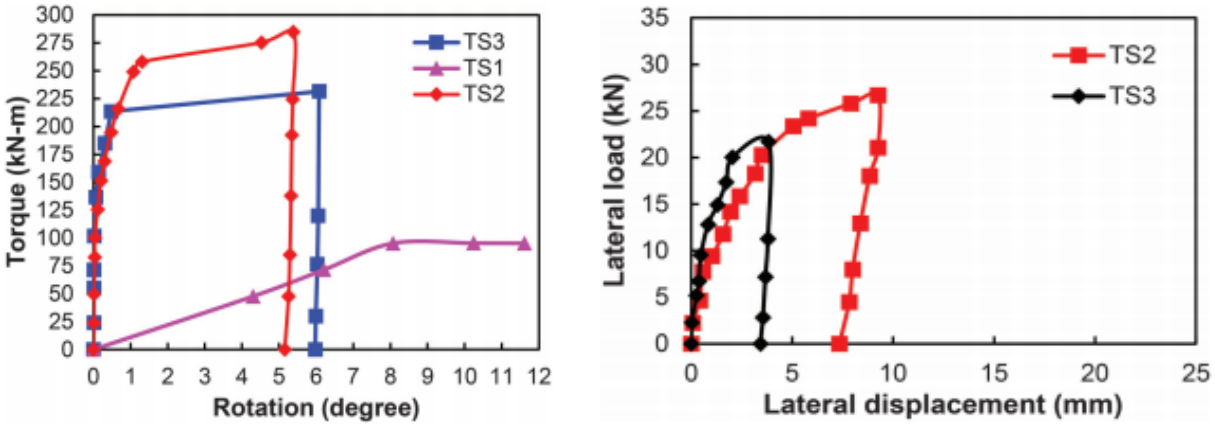

Figure 2.38. Results of the field study by Thiyyakkandi et al. (2016): (a) torque versus rotation; (b) lateral load versus lateral displacement.

CHAPTER 3

Scaled Laboratory Tests

3.1 INTRODUCTION

Torsional and lateral load capacities of piles are functions of several factors, including soil density and pile geometries. To facilitate design and broad implementation of SFPFs, it is necessary to study and understand their torsional, lateral, and combined torsional and lateral load responses in comparison to unfinned piles. Torsional and lateral load capacities of SFPFs and unfinned piles are likely to increase as the soil density increases. The effect of soil density on the torsional capacity of unfinned piles is well understood (see Chapter 2); however, the effect of soil density on the SFPF is relatively unknown and therefore must be carefully studied. Similarly, the increase in lateral load capacity by the SFPF compared to unfinned pile has also been studied extensively. However, the evolution of the soil influence zone for SFPF during lateral loading is not well understood. Selection of pile dimensions and proportions is a critical determination for the study design, as the torsional response of piles is dependent on pile and fin dimensions. Validity of the laboratory test results is also significantly influenced by laboratory test boundary conditions. Test results are valid to the extent that boundary conditions mimic actual, full-scale installations. Therefore, sand particle size, pile dimensions and proportions, and test box dimensions are chosen accordingly, to reduce the effect of boundary condition on the test results.

Based on the study design, a scaled laboratory study was implemented. Detailed explanation of the test setup, engineering drawings, and laboratory test setup photographs are provided in this section. Sand samples were prepared using rainfall method at selected density ranges. The pile installation sequences adopted in the laboratory are also discussed in detail. The section also details the data acquisition system implemented and calculations involved in measuring the pile angular rotation and lateral displacement.

3.2 TEST SOIL PREPARATION

Laboratory tests were conducted in dry, sandy soil, as SFPFs have been demonstrated to be more effective in granular soils (sand and gravel) than in cohesive soils (clay and silt). In addition, laboratory control of soil parameters, including density and homogeneity, of sandy soils is more easily achieved as compared to clayey soils. In the present study, torsional loading, lateral loading and combined torsional-lateral loadings were applied on the piles at low rates. Due to the rapid pore water pressure dissipation in granular materials, tests conducted on dry or moist sand samples will exhibit similar performance and behavior. Therefore, dry sand was used for the laboratory testing.

3.2.1 Soil Properties

Standard F50 Ottawa sand was chosen for this research. The measured properties of Ottawa sand were: mean particle size (D_{50}) = 0.25 mm, coefficient of uniformity (C_u) =1.8, coefficient of curvature (C_c) = 0.95, specific gravity (G_s) = 2.65, maximum void ratio (e_{max}) = 0.78, and minimum void ratio (e_{min}) = 0.48. Direct shear tests suggest the critical state friction angle for the sand was 31.8°. The scanning electron microscope (SEM) image reveals typical subangular shape for the sand particles, as shown in Figure 3.1.

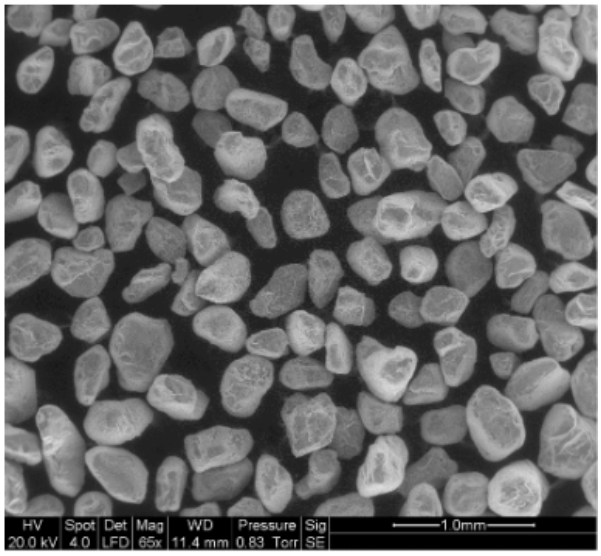

Figure 3.1. SEM image of silica sand used in the present study.

3.2.2 Sample Preparation

Generally, sand is described as loose (D_r = 0-35%), medium (D_r = 35-65%), and dense (D_r > 65%) based on its relative densities. Loose sand in the field is scarce. Therefore, due to limited scope of the present study and lack of studies on torsional tests on SFPFs, torsional tests were carried out in three density ranges, i.e., loose density range (D_r = 20-30%), medium dense density range (D_r = 45-55%), and dense density range (D_r = 75-85%). As it is difficult to find sands with low densities in the field, lateral load tests and combined lateral-torsional load tests were carried out only at medium and dense density ranges. The aim of the combined torsional and lateral load tests was to understand the effect of torsion on the lateral load and vice versa.

Sand deposits were prepared by hand pluviation using a framed #4 sieve and #16 sieves attached to the bottom of the pluviator. The bottom of the pluviator was made of cardboard and holes with 1.58-cm (0.625-in.) diameter were drilled onto the cardboard with a center-to-center spacing of 2.5 cm (1 in.). Based on the target density to be achieved in the tests, different sieve configurations were used. The validity of the calibration curve reported by Kramer et al. (2015) on standard Ottawa sand (Figure 3.2) was tested in the laboratory (Figure 3.3). Kramer et al. (2015) used different sets of sieves and calibrated the fall height of sand, i.e., the distance between the pluviator bottom and sand top, for different target sand densities in the laboratory tests. The height of fall is different for different densities, with large height of fall for higher density. For tests with target relative density of 20-30%, no sieves were attached to the pluviator and the fall height of sand was maintained at a constant distance of 30 cm to achieve uniform sand profile. For achieving a target relative density of 45-55%, a #6 sieve was attached at a distance of 15.24 cm (6 in.) from the pluviator and the fall height was maintained at 30.48 cm (12 in.) (Figure 3.4). For achieving the target relative density of 75-85%, two sieves, #6 and #10, were placed with #6 sieve placed at 15.24 cm (6 in.) below the pluviator and #10 placed at 15.24 cm (6 in.) below the #6 sieve (Figure 3.5). The fall height of sand was maintained at 100 cm (39.37 in.) for achieving the target relative density of 75-85%. The sand bed was first prepared by sand pluviation, where a certain sand volume is allowed to fall from a

predetermined height to prepare the deposit at a certain density. Pluviation is carried out until the sand has completely filled in the sand box.

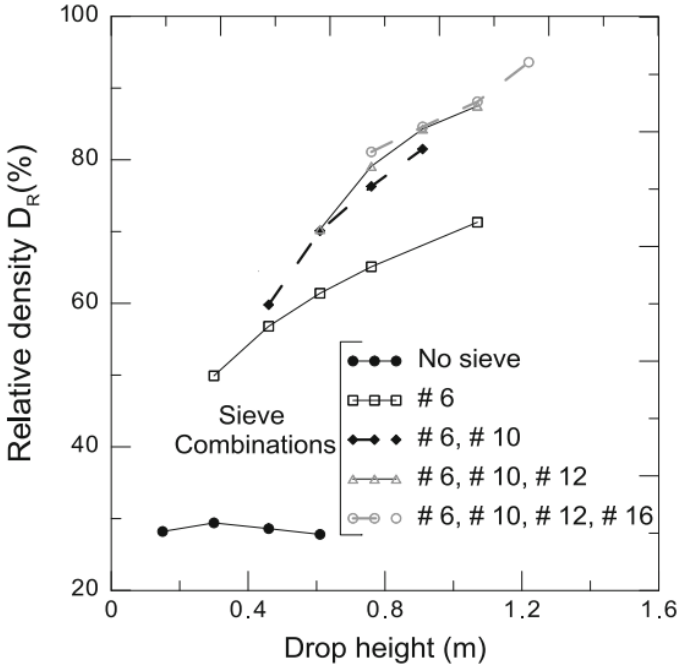

Figure 3.2. Calibration curve reported by Kramer et al. (2015).

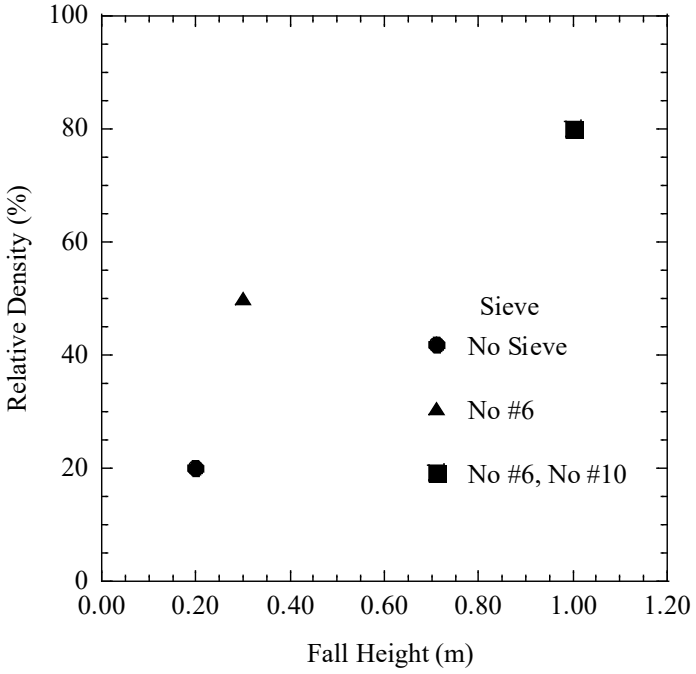

Figure 3.3. Validation of the fall relative density-drop height used in this study.

Figure 3.4. Pluviator including sieves used for preparing dense sand deposits (D_r=75%-85%).

Figure 3.5. Pluviator including sieves used for preparing medium dense sand deposits (D_r=45%-55%).

3.3 TEST SETUP

The present section provides the detailed explanation of test setup components used in the present study. Figure 3.6 presents the laboratory test setup. Laboratory tests were carried out in a cast iron box with dimensions of 1.8 m (70.8 in.) × 1.8 m (70.8 in.) × 1.2 m (47.25 in.). The steel frame consisted of four steel plates bent in the form of C sections.

For the torsional tests, a steel wire rope sling cable of 3.11-mm (1/8-in.) diameter was attached to the pile using a pile head. The pile was loaded under gravity loading using a loading pan. The steel wire applies lateral and torsional loading on the pile, due to the loading eccentricity provided by the pile head. Torsional loading was achieved by using a steel rod connected to the pile and pile head (see Figure 3.7). Bush connections were provided at the joints between the horizontal C sections and the steel rod. The bush connections provided translational fixity to the pile while pile rotation was unrestricted.

For the lateral load tests, the steel rod connected to the pile was removed after the pile installation sequence. A steel wire rope of 3.11-mm (1/8-in.) diameter was attached on top of the pile at a distance of 10 cm from the top of the fin. The pulley mechanism was adjusted to provide a lateral load on the pile. For the combined lateral and torsional loading tests, after installation of piles into the sand, the steel rod was removed. A pile head with two steel plates welded to the top and bottom of the pile head as shown in Figure 3.8 was installed on top of the pile using pins. Holes of 0.635-cm (¼-in.) diameter were drilled in the rectangular plates at 7.5 cm, 15 cm, and 30 cm from the center of the pile head. For applying combined lateral and torsional load, at any arm length, a pin with 0.635-cm (¼-in.) diameter was inserted in the hole and a steel wire rope of 0.315-cm (1/8-in.) diameter was attached to the pin. The load was applied using the loading pan. A detailed description of each of these test components is discussed in the subsequent sections.

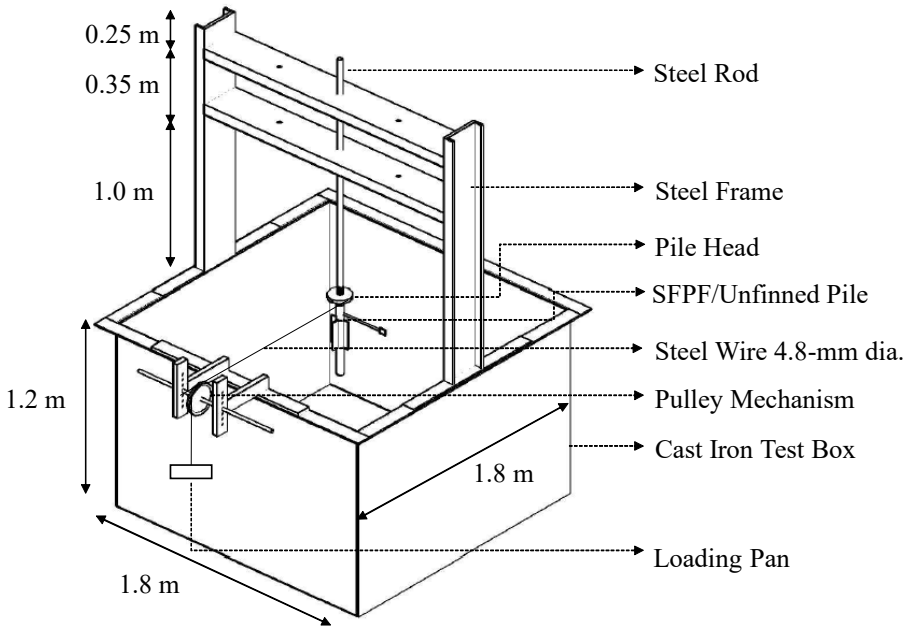

Figure 3.6. Diagram of laboratory test setup (not to scale).

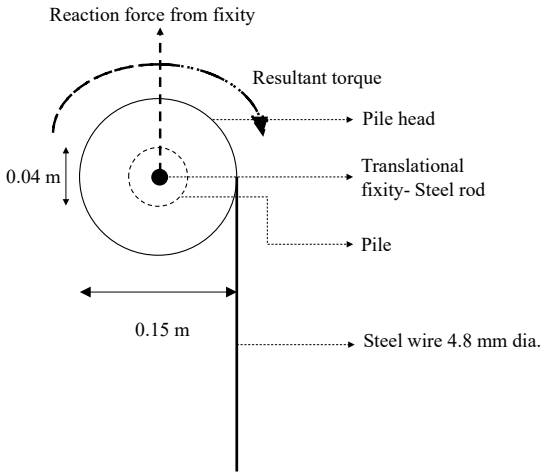

Figure 3.7. Loading mechanics for tests including the direction of resultant translational load and torque for torsional tests.

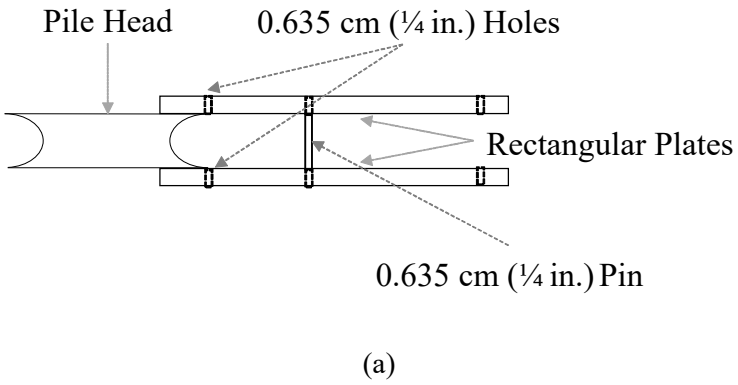

(a)

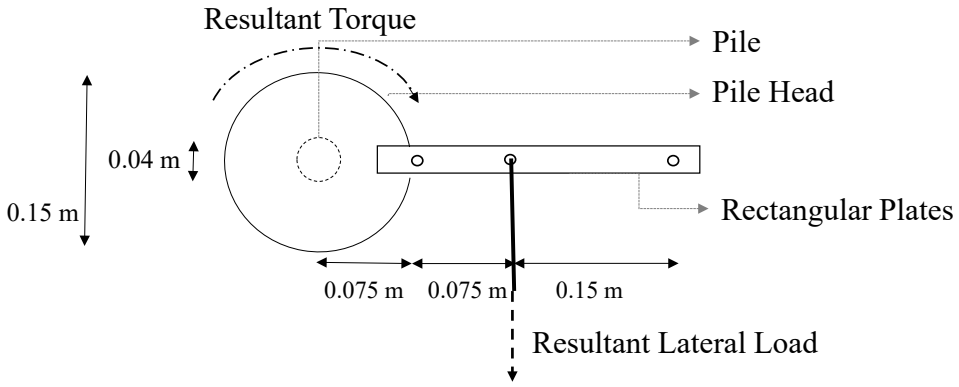

(b)

Figure 3.8. Loading mechanics for the combined torsional and lateral load tests: (a) section view; (b) plan view including the direction of resultant translational load and torque for torsional tests.

3.3.1 Test Box

The laboratory tests were carried out in a cast iron box with dimensions 1.8 m (70.8 in.) × 1.8 m (70.8 in.) × 1.2 m (47.25 in.) (see Figure 3.9). The sides of the box were made smooth to reduce the effect of friction on test results. The sides of the box have plates with 0.089 m width to attach the test frame.

Figure 3.9. Test box used for laboratory study.

3.3.2 Test Frame

The test frame consisted of two vertical C sections and two horizontal C sections (see Figure 3.10). The vertical C sections had a width of 6.95 cm (2.739 in.), a depth of 25.4 cm (10 in.), a thickness of 0.96 cm (0.379 in.), and a length of 1.6 m (63 in.), while the two horizontal C sections had a width of 6.95 cm (2.739 in.), a depth of 25.4 cm (10 in.), a thickness of 0.96 cm (0.379 in.), and a length of 1.8 m (70.9 in.). Vertical C sections were attached on a rectangular steel plate (120 cm × 1 cm × 0.1 cm) and the steel plate was attached to the test box using 1.9-cm (¾-in.) diameter bolts. The horizontal C sections were attached to the vertical C sections at 1 m (39.4 in.) and 1.35 m (53.1 in.), respectively.

The heights of the horizontal sections were chosen in order to fit the pile length between the sand deposits and the lowest horizontal member so that piles could be driven into the sand after deposition. Bush connections were provided at the joints between the horizontal C sections and the steel rod (½-in. diameter) such that the connections were aligned vertically. The bush connections provided translational fixity to the piles, while pile rotation was unrestricted.

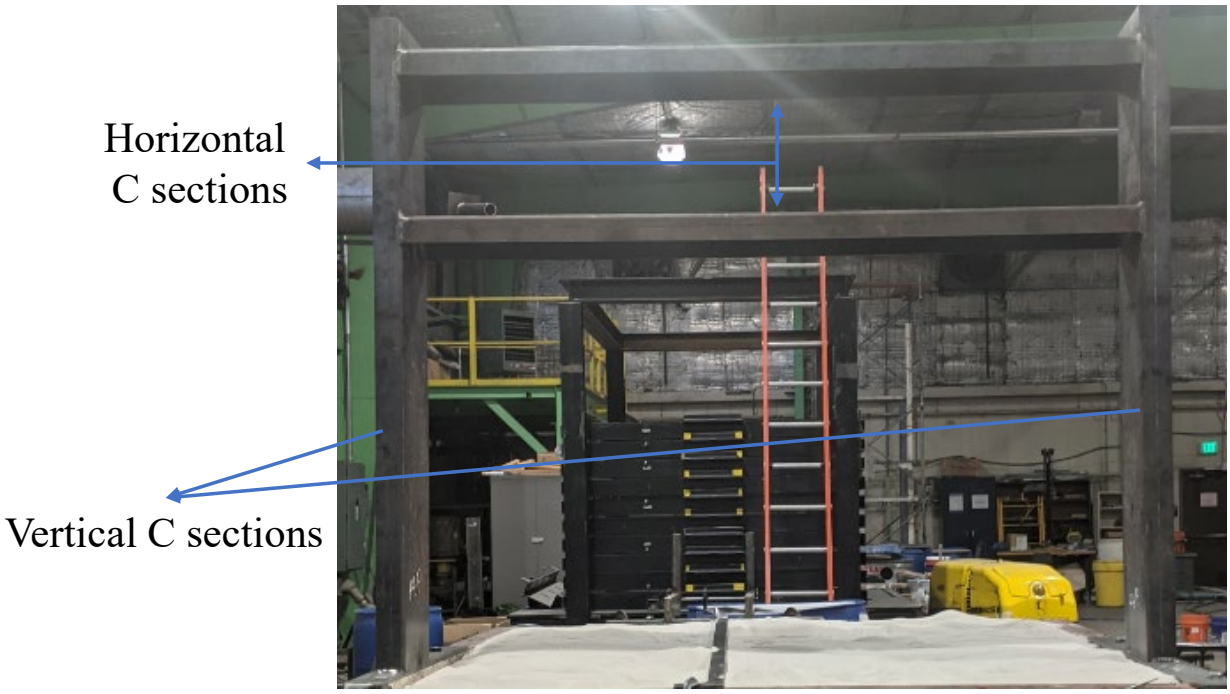

Figure 3.10. Frame used for the tests.

3.3.3 Unfinned Pile and SFPF

The SFPF dimensions and proportions used for laboratory testing were chosen such that the SFPF provides maximum lateral load resistance. Lateral load resistance is the limiting criterion for SFPF design. Accordingly, W_F/D_P and L_F/L_P were chosen from literature to be 1 and 0.5, respectively. The same diameter (D_P) and pile length (L_P) were chosen for SFPF and unfinned piles to provide a direct comparison between pile torsional capacities.

The piles considered in the present study had total and effective lengths of 50 cm (19.7 in.) and 36 cm (14.2 in.), respectively. Effective length is defined as the pile length embedded in sand and providing torsional resistance. Outer and inner pile diameters were 40 mm (1.57 in.) and 38 mm (1.5 in.), respectively. For the pile diameter and length considered, optimum fin length and width of 180 mm (7.09 in.) and 40 mm (1.57 in.) were chosen such that the pile provides maximum lateral load capacity. Fins were made using 1.6-mm-thick steel plates. The pile dimensions were chosen to be the same as those used by Abongo (2019) in their lateral load tests. A rectangular four-fin configuration with fins placed at the pile top was used in the SFPF. The pile dimensions used for the present study are shown in Table. 3.1.

Table 3.1. Pile dimensions used in the present study.

Length of Pile (L_P)	36 cm (14.17 in.)
Diameter of the Pile (Outer Diameter) (D_P)	4 cm (1.57 in.)
Thickness of Pile and Fins	0.16 cm (0.039 in.)
Width of Fins (W_F)	4 cm (1.57 in.)
Length of Fins (L_F)	18 cm (7.08 in.)

A 15.24-cm (6-in.) diameter, non-bearing pulley (McMaster Carr Model No. 3164) was attached on top of the piles to provide the necessary eccentricity to the applied loading. The steel rod used for pile driving and torsional loading was attached to the non-bearing pulley and pile using a pin. A steel L hook (½ in. × 8 in. × 2 in. × 2½ in., McMaster Carr Model No. 91587A210) was welded onto the non-bearing pulley.

A cylindrical arm (0.635-cm [1/2-in.] diameter steel rod) of 30 cm (11.8 in.) length was welded to the piles at 45 cm (17.7 in.) height (see Figure 3.12). The arm was attached with a rectangular steel plate (3 cm × 3 cm × 0.16 cm) at its end. The dial gauge, measuring the angular rotation, was positioned such that the gauge head was in contact with the rectangular plate while the gauge head of the dial gauge measuring the lateral displacement was kept in contact with the pile. Figures 3.11 and 3.12 show the piles used for the laboratory tests.

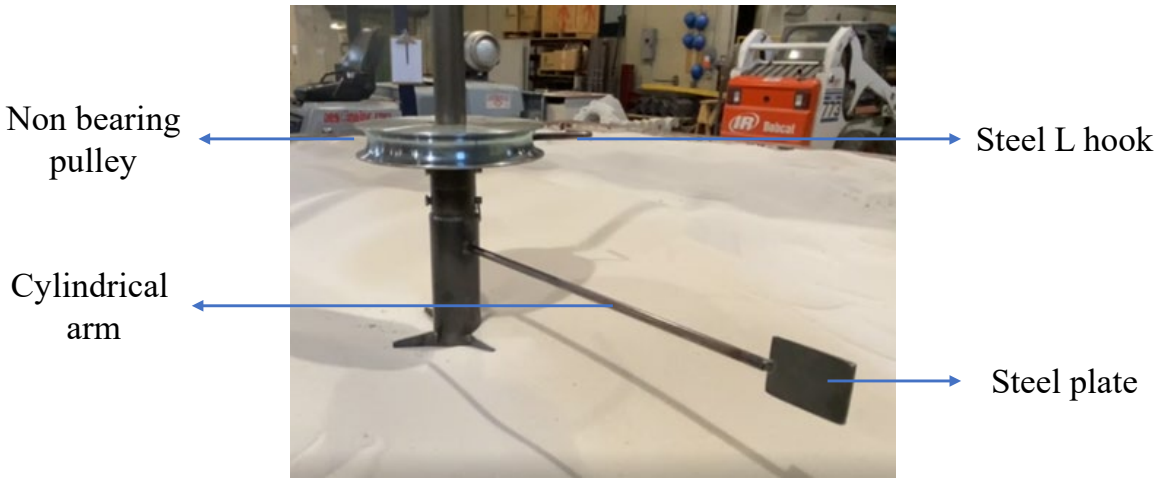

Figure 3.11. SFPF with the cylindrical arm and rectangular plate.

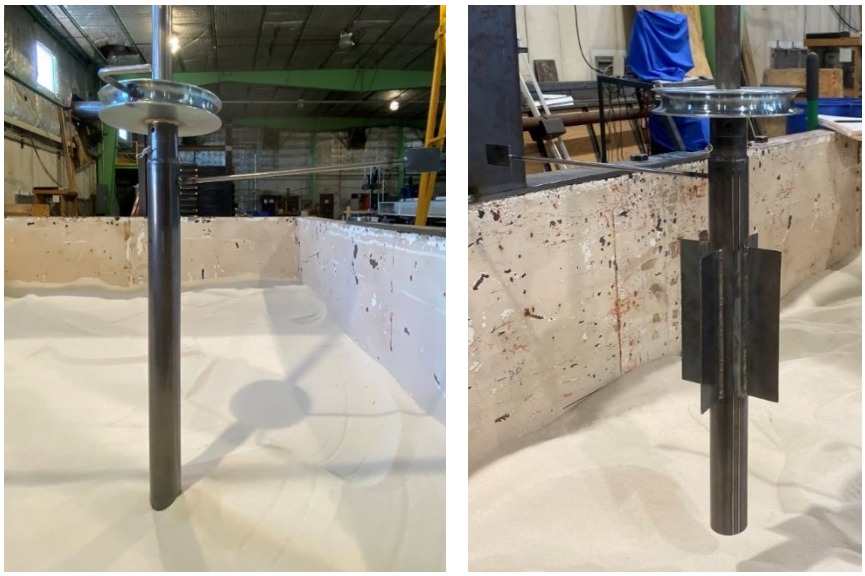

Figure 3.12. Piles tested in the laboratory: (a) unfinned pile; (b) fin pile.

3.3.4 Data Acquisition

Torsional loading, lateral loading, or combined both loadings were applied on the piles using the loading pan and pulley mechanism. The rigid steel arm length L used for measuring the angular rotation in the present study is 30 cm (11.8 in.).

Dial Gauge

Dial gauges with magnetic-base holder were used to measure angular rotation and lateral pile displacement. The dial gauges used for the study are Mitutoyo model number 2424S-19 (Figure 3.13). The dial gauge has a continuous dial numbered clockwise around the face for direct measurements and the gauge head retracts and extends to measure deformation. Maximum travel distance for the dial gauge used in the present study was 5 cm (2 in.) and the least count of measurement was 0.00254 cm (0.001 in.). Dial reading was subdivided into 100 readings and, therefore, during each rotation dial gauge measures 0.254 cm (0.1 in.). As noted in the literature, the increase in torque magnitude at low angular displacement ($\sim 0.01^o$- 0.5^o) is high. Therefore, to capture these low angular displacements, dial gauges with 0.025-mm (0.001-in.) least count was used in the present study. Using this dial gauge, the lowest angular rotation of 8.5×10^{-5} rad ($\sim 0.005^o$) could be measured. During torsional loading, arc rotation (Δ) of the rigid steel arm of known length (L), attached to the pile, was measured using a dial gauge. For small arc rotations (Δ), angular displacement (θ) was calculated using

$$\theta = \frac{\Delta}{L} \tag{3.1}$$

For combined lateral and torsional loading, two dial gauges were used, one to measure the lateral displacement (δ) and the other to measure the pile angular rotation. Angular rotation is derived from the dial gauges using basic geometry.

Figure 3.13. Mitutoyo dial gauge model 2424S-19, 5-cm (2-in.) travel, LC 0.00254 cm (0.001 in.).

3.3.5 Pulley Mechanism

The pulley mechanism consisted of two L-shaped heavy-duty steel bars. The steel bars extended 0.3 m and had a height of 0.3 m (see Figure 3.14). The bars were welded to a steel plate having dimensions 1.2 m × 0.09 m × 0.02 m. The steel plate was attached to the test box using 1.9-cm (¾-in.) bolts. The vertical portion of both the L-shaped bars was drilled with holes of 1.27-cm (½-in.) diameter at different elevations to adjust the pulley to apply load. A steel rod (0.635-cm (1/4-in.) diameter) was inserted in the vertical L section at any height such that the loading applied on the pile was horizontal. The pulley used for the present study (McMaster Carr model no. 3628T11) had an outside diameter of 5.715 cm (2¼ in.), shaft diameter of 0.9525 cm (3/8 in.), and width of 2 cm (13/16 in.).

For torsional loading, the piles were loaded using the steel wire attached to the pile head. The steel wire passes over the pulley mechanism and is attached to a pan used for loading. The pile head provides an eccentricity of 7.5 cm. For combined torsional and lateral load tests, steel wire was used to load the pile at different eccentricities of 7.5 cm, 15 cm, and 30 cm. Weight in the loading pan, multiplied with the eccentricity (7.5 cm), provided the applied torque.

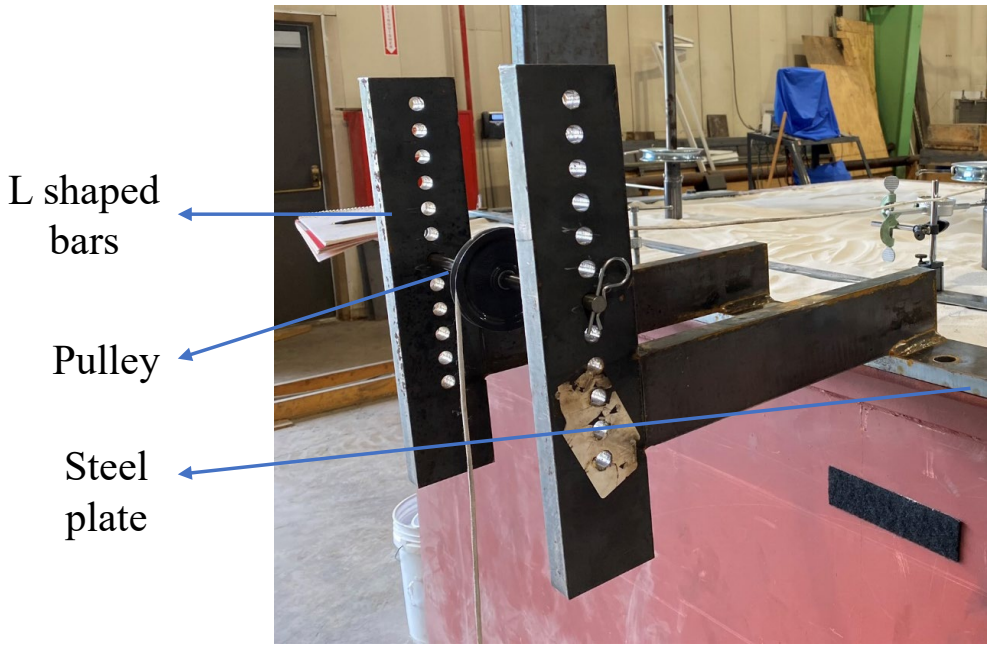

Figure 3.14. Pulley mechanism.

3.4 PROCEDURE

The test frame was securely mounted on the test box using 1.9-cm (¾-in.) diameter steel bolts. Sand deposits were prepared using the pluviator. Depending on the D_r of the deposits to be prepared, the fall height of sand was determined from Figure 3.7. The fall height for 15%-20%, 45%-55%, and 75-85% D_r was obtained to be 20 cm, 30 cm, and 100 cm, respectively. Steel rods were mounted and secured on the test frame at the designated locations where piles were installed (Figure 3.15(a)). The SFPF and unfinned pile were connected to the steel rods using pins. In the field, piles are generally installed in sandy soils using vibration. The pile is attached to the vibrator and a vertical vibratory force is applied from the top, thus penetrating the pile into sand. In this experimental study, SFPF and unfinned piles were driven into the soil following a similar methodology adopted in the field. The steel rod was driven into the sand using a rotary drill hammer until the top of the effective pile length coincided with the top of the box (Figure 3.15). The rotary hammer drill had an input current of 11 amp and impact energy of 11.4 Joules (8.4 ft-lb), which imparts 1,200 blows per minute on the steel rod, replicating the pile-driving mechanism in the field. The pile driving is continued until the predetermined pile length is embedded in sand. For lateral load tests and combined lateral plus torsional load tests, the steel rod was removed after the pile installation.

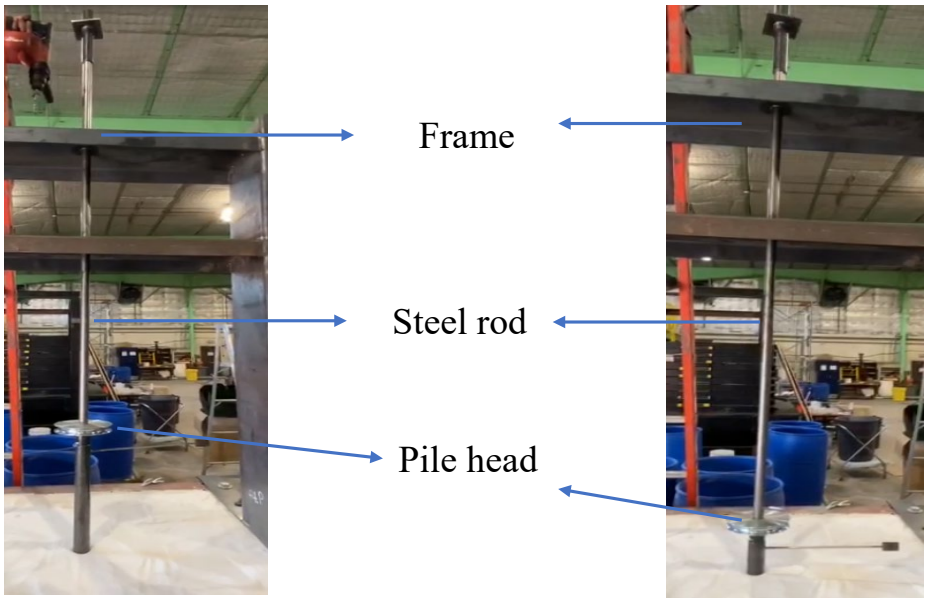

Figure 3.15. Installation of unfinned piles in the laboratory: (a) before installation; (b) after installation.

After pile installation, a rectangular steel bar with dimensions 1.8 m × 0.05 m ×0.01 m was rigidly attached to the box for mounting the magnetic base of dial gauges. The steel bar was attached on the test box, parallel to the test frame. Dial gauges mounted on the steel bar were used to measure the lateral displacement and angular pile rotation. For the torsional tests, two dial gauges were mounted on the steel bar as shown in Figure 3.16. The dial gauge at the steel plate measured the angular rotation while the dial gauge on the pile checked for any lateral movement of the pile. For lateral load tests, the dial gauge was attached to the pile at a height of 5 cm from the sand surface as shown in Figure 3.17. For combined lateral and torsional loading, two dial gauges were mounted (see Figure 3.18). The magnetic mounts had adjustable bars, which were used to adjust the dial gauge positions. Before each test, a grid with squares of size 1.6 cm (0.63 in.) was imprinted on the sand and monitored during the test using a high-speed camera from above to investigate the influence zone (see Figure 3.19).

Figure 3.16. Data acquisition setup for torsional load tests.

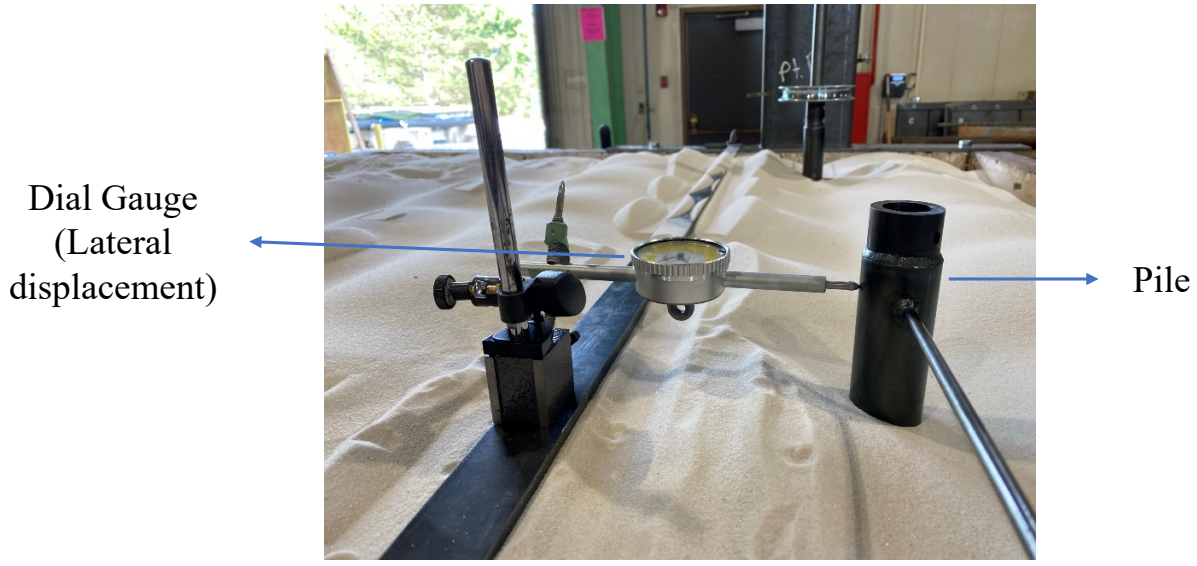

Figure 3.17. Data acquisition for lateral load tests.

Figure 3.18. Combined torsional and lateral load test setup loaded at an arm length of 15 cm.

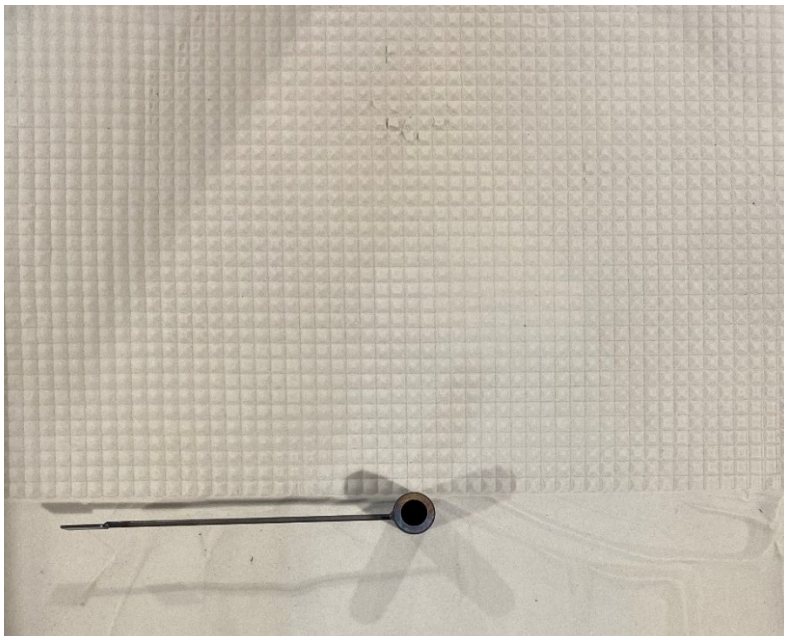

Figure 3.19. Initial position of the mesh imprinted on dense sand deposits.

For torsional tests, after sand deposition, a 0.3175-cm (1/8-in.) diameter steel wire was attached to the pile head using the welded L hook on the pile head. The steel wire was wrapped around the pile head and went over the pulley mechanism (see Figure 3.20). A pan was placed at the end of the steel wire to load the pulley. A frictionless pulley was used to reduce the frictional loss. A load of 0.5 N was applied on the pulley and the torque applied on the pile was calculated by multiplying the moment arm with the load. Incremental loading of 0.5 N was applied on the pile until large lateral displacements or angular rotations occurred in

the piles. Dial gauge readings were recorded for each load increment. Sufficient time was provided between each incremental loading to eliminate the effect of loading rate on the response obtained.

Figure 3.20. Pile after installation.

For torsional tests, after pile installation, loading was applied using the pulley mechanism. An eccentricity of 75 mm was provided by the pile head. Pile was loaded using small weights, each weighing 50 g (0.5 N), until considerable angular displacement had occurred in the piles. Weight in the loading pan, multiplied with the eccentricity, provided the applied torque on the pile. For lateral load tests, after pile installation, loading was applied using the pulley mechanism. The dial gauge measuring the lateral displacement was placed at 50 mm from the top of the fins on the pile. It is evident from the literature that the pile rotates at a depth of 0.72 L_P from the surface. Therefore, the lateral displacement measured from the dial gauge was converted into lateral pile head displacement using simple geometry. Lateral load was applied in increments of 500 g (5 N) until considerable lateral displacement had occurred in the pile. For the combined torsional and lateral load tests, after pile installation, the pile head with the rectangular plates was attached on the pile. Three eccentricities of 7.5 cm, 15 cm, and 30 cm were used in this study and according to the eccentricity chosen, a 0.635-cm (¼-in.) pin was inserted and the pin was pulled using the steel wire. For the eccentricity chosen, an incremental load of 500 g (5 N) was applied using the pulley mechanism. The torque was calculated by multiplying the eccentricity with the load, similar to the methodology used in the torsional tests. The test was carried out until considerable angular rotation/lateral displacement had occurred in the pile.

Results are reported in terms of torque applied (τ), angular displacement (θ), lateral load (P), and lateral displacement at pile head (δ). For torsional tests, τ versus θ is plotted and for lateral load tests, P versus δ

is plotted. For combined lateral and torsional load tests, τ versus θ and P versus δ are plotted. An arbitrary rotational displacement (θ_o) is used as the failure criterion for the torsional test. For lateral load tests, the tests were conducted until a normalized lateral displacement of 0.2× D_P had occurred on the pile head. For the combined lateral and torsional loading, rotational displacement (θ_o) criterion or lateral displacement (δ_o) criterion, whichever was reached first, was used as the limiting criterion.

3.5 BOUNDARY EFFECTS AND TEST CONFIGURATION

Test box dimensions and test configurations were chosen such that the influence of boundary on the test results was minimized. As noted by Abongo (2019), side walls of the test box are made smooth to minimize wall friction. Grain size distribution of the sand used in the present study was chosen such that the ratio of pile diameter (D_p) to mean grain size of sand (D_{50}) was greater than 30, hence eliminating the particle size scale error (Franke and Muth 1985).

The test configuration was determined based on the pile influence zone during testing. As the lateral load tests dictated the size of the influence zone in the tests, the experimental configuration was determined based on the lateral load tests. Studies by NCHRP (2011) showed that the influence zone during lateral loading is 4×D_p along the loading direction, while the strain wedge measured by Hajialilue-Bonab et al. (2013) showed that the influence zone extends to a distance of 5.5×D_p. Abongo (2019) carried out tests on unfinned piles and fin piles and showed that even at high lateral displacements, the influence zone is within 12D_p.

Based on the boundary conditions illustrated, the test configuration with test box dimension is shown in Figure 3.21. Torsional tests on unfinned piles and fin piles were carried out first. After each test, the pile was removed and driven in the next location, where lateral load tests were carried out, as shown in Figure 3.21. After the torsional and lateral load tests, the sand was removed and pluviated again to the required density and the combined torsional and lateral load tests were conducted.

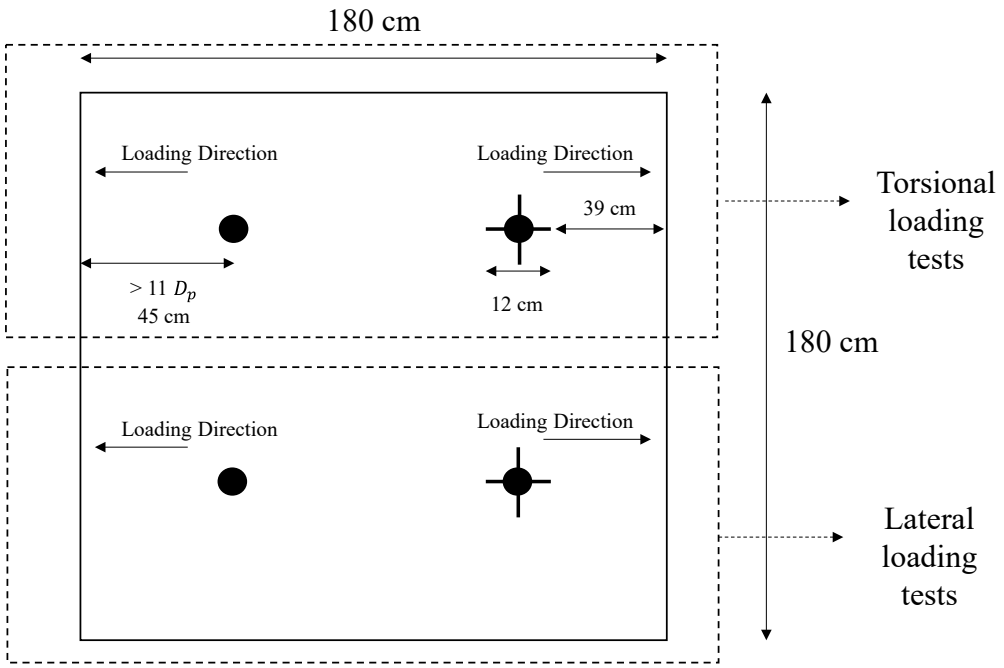

Figure 3.21. Plan view of test configuration including dimensions.

SUMMARY

This chapter presents the variables chosen for the laboratory studies on SFPFs and unfinned piles. Sand deposits for the tests were prepared at different relative densities, representing medium and dense conditions. Three density ranges were considered for torsional tests while two density ranges were considered for lateral load tests. The SFPF dimensions and proportions, providing maximum lateral load capacity, were used. Test results on SFPFs were compared with unfinned piles to obtain a direct comparison between the tests. Test box dimension and test configuration were decided based on the pile influence zone during torsional or combined torsional and lateral load testing, to reduce boundary influence on the test results. The chapter also provides the detailed procedure followed in the laboratory tests along with the calculations.

CHAPTER 4

Experimental Test Results

4.1 INTRODUCTION

This chapter presents the results of the laboratory experiments carried out on SFPFs and unfinned piles. Key results in this chapter include:

- Torque versus angle of rotation response of SFPFs compared with unfinned piles for different sand relative densities.
- Lateral load versus normalized lateral displacement response of SFPFs compared with unfinned piles for different sand densities.
- Development of influence zone in SFPFs and unfinned piles during lateral loading.
- Effect of arm length on the torsional and lateral load capacities of SFPFs.

4.2 TORSIONAL RESISTANCE OF UNFINNED PILES AND SFPFs

4.2.1 Torque versus Rotation

As the fin piles are generally used for offshore wind turbine foundations, most of the studies in the literature concentrated on the lateral load tests on fin piles and did not consider torsional loading. In the present study, torsional test results are reported first. Generally, failure is deemed as the point where large rotation occurs for small increments of torque applied. However, this criterion might be satisfied only at very large rotation angles, which can exceed the service limit of these foundations. Therefore, in this study, the limiting criterion used by Zhang and Kong (2006) was used where the failure angle (θ_f) is a function of the applied torque (T) and is given by

$$\theta_f = \frac{180\,TL_P}{\pi\,G\,I_P} + C \tag{4.1}$$

where G is the shear modulus of the pile, I_P is the polar moment of inertia of the pile, and C is the toe twist angle at failure. Zhang and Kong (2006) noted the value of C to be 3^o. The first term in Equation 4.1 takes into account the twist in the pile and, for the length of the pile considered in the present study, the twist is calculated to be on the order of 10^{-8} degrees and hence is negligible. This tends to make the value of θ_f constant for the assembly of piles considered.

The repeatability of the torsional experiments was studied by carrying out two torsional tests on SFPF on dense sand deposits prepared at the same density. Figure 4.1 shows a comparison of the torque versus rotation curves obtained from the experiments, and the excellent agreement suggests good test repeatability.

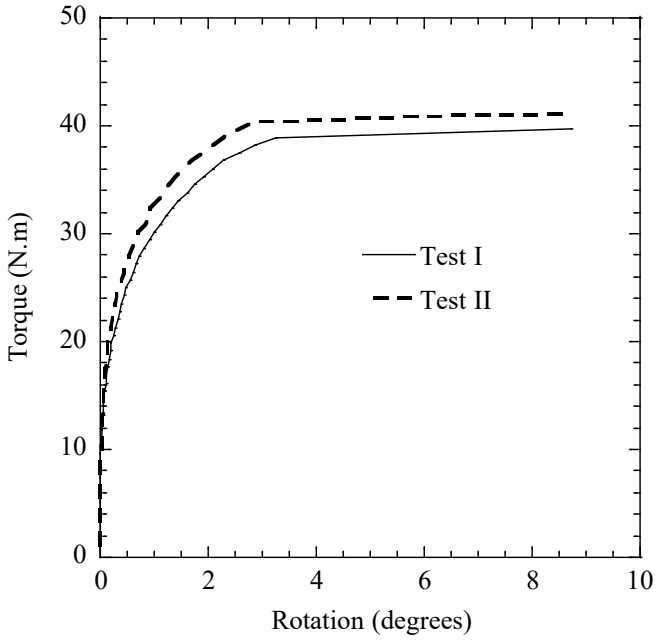

Figure 4.1. Torque vs. rotation for SFPFs in dense sand.

Figures 4.2 and 4.3 show the torque-rotation curves of the unfinned piles and fin piles with the tests conducted until failure, i.e., there is a significant increase in rotation without additional torque applied. Figures 4.1 and 4.2 also show the limiting failure line of 3^o chosen according to Zhang and Kong (2006). Even though there are no criteria mentioned in the manuals of DOTs, it is reasonable to assume failure at a rotation of 3^o, as beyond this the rotation can significantly affect the functionality of the structures.

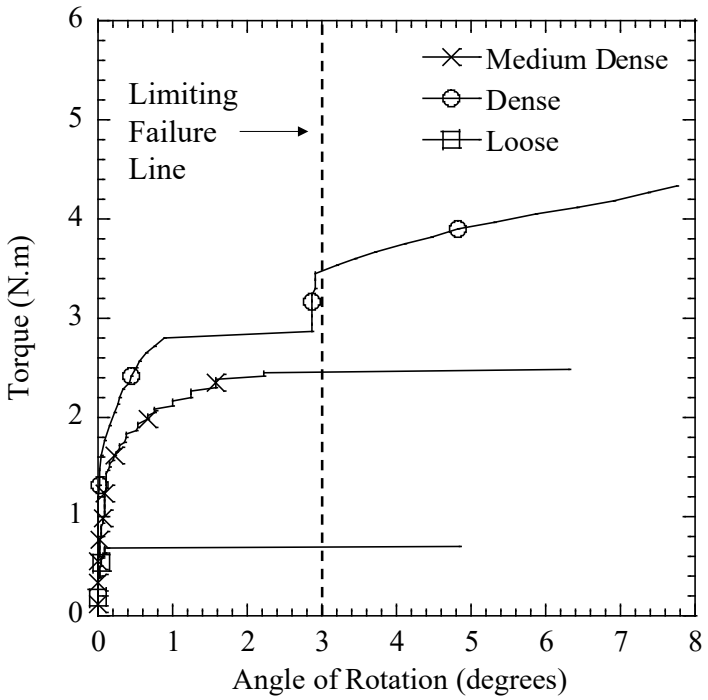

Figure 4.2. Torque vs. rotation for unfinned piles in loose, medium dense, and dense sand.

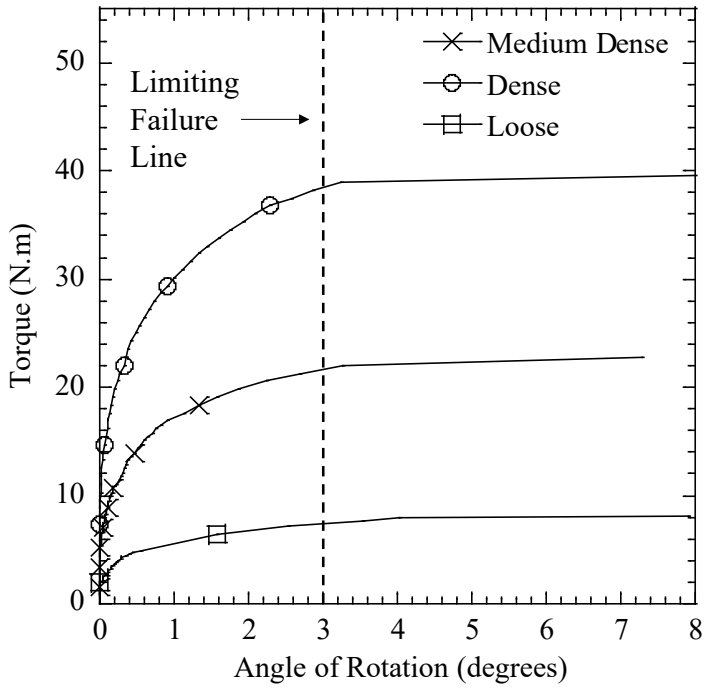

Figure 4.3. Torque vs. rotation for SFPFs in loose, medium dense, and dense sand.

From Figures 4.2 and 4.3, it is evident that for unfinned piles and SFPFs, the torsional capacity increases with an increase in the sand relative density. For unfinned piles, failure occurs at a very small angle of rotation. The pile suddenly slips, leading to large angular rotations. However, this type of failure is not observed in SFPFs, where failure is more gradual and even at large angles of rotation, the pile did not undergo slippage.

4.2.1 Fin Efficiency versus Rotation

The performance of SFPFs can be quantified using torsional efficiency (η_T), which is defined as the increase in torsional resistance at a particular angle of rotation for a SFPF in comparison to the corresponding unfinned pile. The equation for calculating η_H is shown below:

$$\eta_T = \frac{T_F - T_M}{T_M} \tag{4.2}$$

where T_F and T_M are the torque corresponding to the rotation considered for the SFPF and unfinned pile, respectively. Figure 4.4 presents the torsional efficiency versus pile rotation for the SFPFs in loose, medium dense, and dense sand deposits. From Figure 4.4, it is noted that the sand relative density plays an important role in the pile efficiency under torsional loading. Generally, for a given relative density, the efficiency slightly increased with rotation. The SFPF efficiency is similar for the loose and medium dense sands and is the highest in the dense sand.

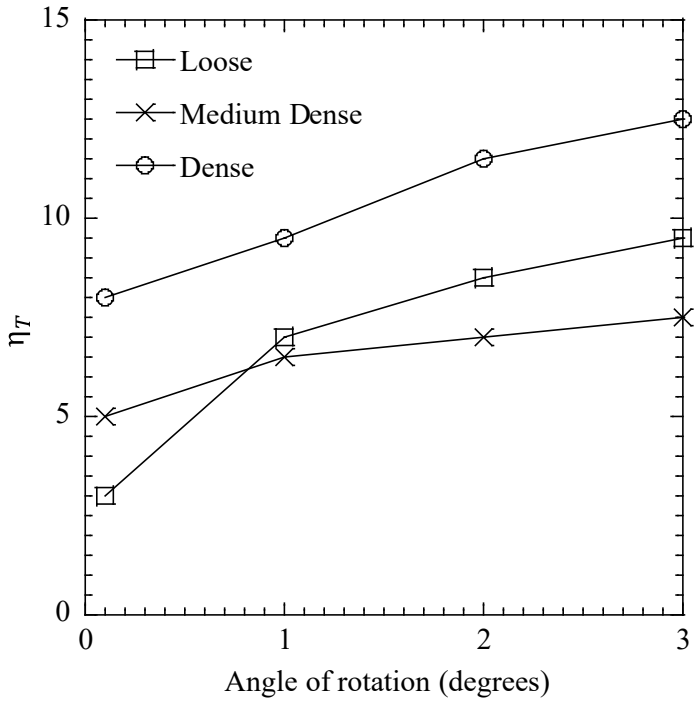

Figure 4.4. Torsional efficiency of SFPFs vs. angle of rotation.

4.3 LATERAL LOAD TESTS ON UNFINNED PILE AND SFPFs

4.3.1 Lateral Load versus Normalized Lateral Displacement

PennDOT (2011) and Oregon DOT (2018) specified a lateral movement of 2.54 cm (1 in.) as the limiting lateral pile head displacement. Sawwaf (2006) and Peng et al. (2011) used a pile head displacement of 10% to 20% of D_p as the failure criterion, while Abongo (2019) used 20% of D_p. The lateral load-carrying capacity of unfinned piles and SFPFs in the present study was evaluated at a load resulting in a pile head lateral deflection equal to 20% of D_p (i.e., 8 mm/0.31 in.) based on the scaled pile geometry to accommodate a wide range of applications. It is evident from the literature that the point of rotation of the SFPF and unfinned piles during lateral loading is approximately at 0.72 L_p from the ground surface (Abongo 2019). Therefore, the displacements obtained from the lateral LVDT placed at 50 mm above the pile head can be converted into the pile head deformations.

The repeatability of the lateral load test results was evaluated by carrying out two lateral load tests on SFPF in dense sand deposits. Figure 4.5 shows a comparison of the test results in terms of lateral load versus normalized lateral displacement (y/D_p), and the excellent agreement suggests good test repeatability.

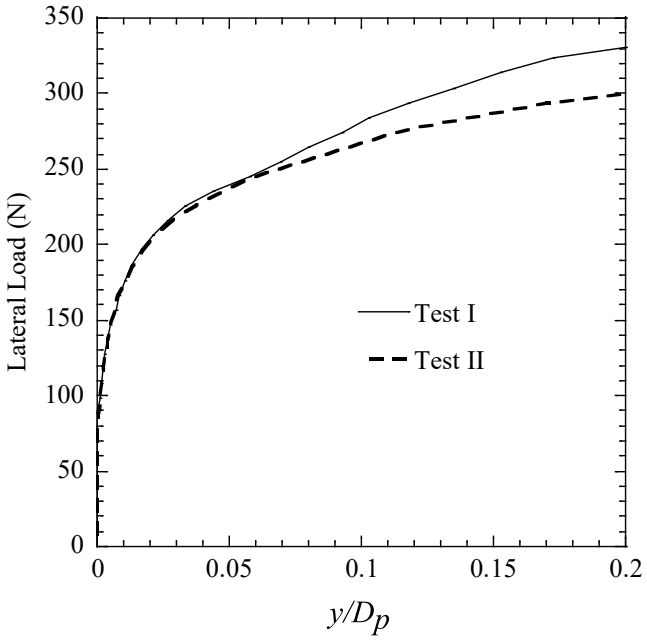

Figure 4.5. Torsional efficiency of SFPFs vs. angle of rotation.

In this section, lateral load tests were carried out on piles and the results are reported until the lateral displacement of the pile head is 20% of D_p. The results are reported for unfinned piles and SFPFs installed in the medium dense and dense sand deposits. The lateral load applied on the pile versus pile head displacement normalized by D_p is plotted in Figure 4.6. The effect of sand density is clearly evident, as the pile capacity increases significantly as the sand density increases. For unfinned piles in the dense sand, at a normalized displacement of 20% of D_p, the capacity is increased 2.5 times compared to the unfinned piles in medium dense sand at the same displacement. The effect of fin is also evident in Figure 4.6, as the fins increase the lateral load capacity significantly. The slopes of the lateral load-displacement curves for all the

piles considered in this study are high initially but become significantly smaller at high displacements as the strength in the soil is completely mobilized. To understand the repeatability of the test and uniformity of the specimens prepared using the pluviator, additional lateral load tests were carried out on SFPF in the dense sand deposits. The lateral load versus normalized lateral displacement is plotted and the results are compared with the results of the corresponding test reported in Figure 4.6. Lack of significant variation between the two tests shows that the preparation methodology adopted can be used to obtain uniform sand deposits and the repeatability of the test is also noted.

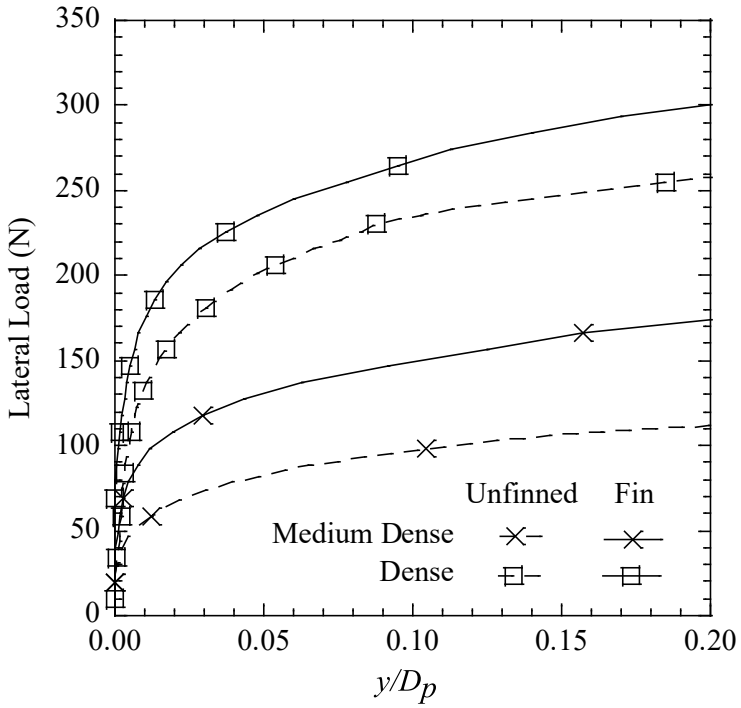

Figure 4.6. Lateral load vs. normalized lateral displacement.

4.3.2 Fin Efficiency versus Lateral Displacement

The performance of SFPFs can be evaluated using load efficiency (η_H), which is defined as the increase in lateral resistance at pile head at a particular lateral displacement for a SFPF in comparison to the corresponding unfinned pile. The equation for calculating η_H is shown below:

$$\eta_H = \frac{H_F - H_M}{H_M} \tag{4.3}$$

where H_F and H_M are pile head lateral load of SFPF and unfinned pile, respectively. Figure 4.7 presents load efficiency versus pile head lateral displacement for the SFPFs in the medium dense sand and dense sand.

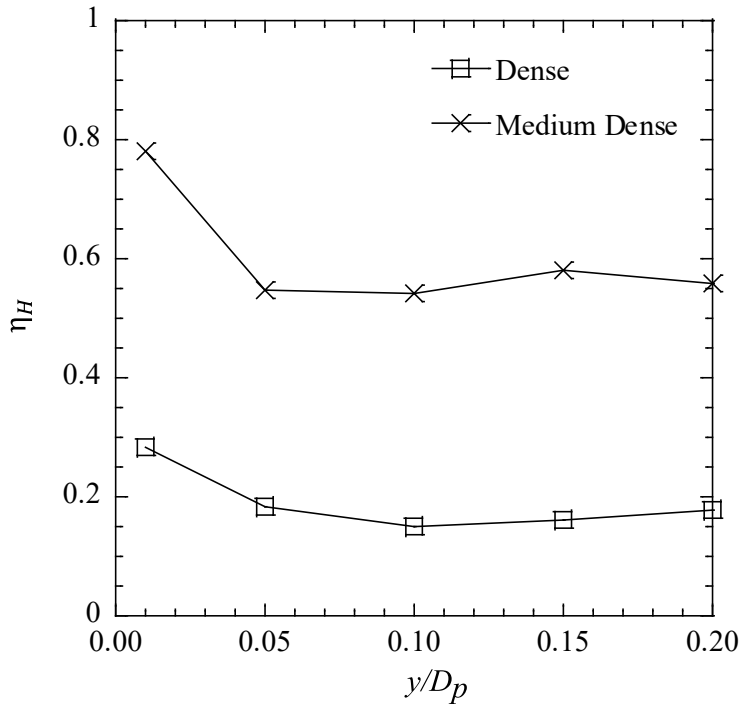

Figure 4.7. Lateral load efficiency of SFPFs versus normalized lateral displacement.

From Figure 4.7, it is clear that the effect of fin in increasing the lateral load-carrying capacity is most significant at low displacements (i.e., low load level). With an increase in lateral pile movement, the efficiency decreases significantly until a certain pile head displacement ($y/D_P \approx 5\%$). Beyond this point, the efficiency remains constant irrespective of the pile head displacement. The constant values of η_H are noted to be 0.55 for the medium dense sand deposits and 0.18 for the dense sand deposits. Therefore, it can be concluded that for pure lateral loading, the SFPFs significantly improve the lateral load capacity in the medium dense sand compared to the dense sand. The results are in general agreement with those reported from the field study of Murphy et al. (2016).

4.3.3 Length and Width of Strain Wedge for Unfinned Pile and SFPF

The length, width, and shape of the influence zone need to be accurately measured to obtain the lateral load resistance of unfinned piles and SFPFs. In this section, the length, width, and shape of the failure zone for unfinned pile and SFPF are discussed. Abongo (2019) used pressure cells at different positions to obtain the failure zone in sand at different pile head displacements. In this study, a simpler approach was used. The sand tested was imprinted with grids, and the movement of the grids was monitored during the tests. The test on SFPF in dense sand was carried out to large lateral strains and at a normalized lateral displacement (i.e., y/D_P) of 100%, the failure wedge is shown in Figure 4.8. The length of the failure zone (L_f) and width of the failure zone (W_f) are also shown in Figure 4.8. Length of the strain wedge is taken as the distance from the center of the initial position of the unfinned pile or SFPF to the horizontal grid that is disturbed, while width of the influence zone is the distance between the outer most disturbed vertical grids.

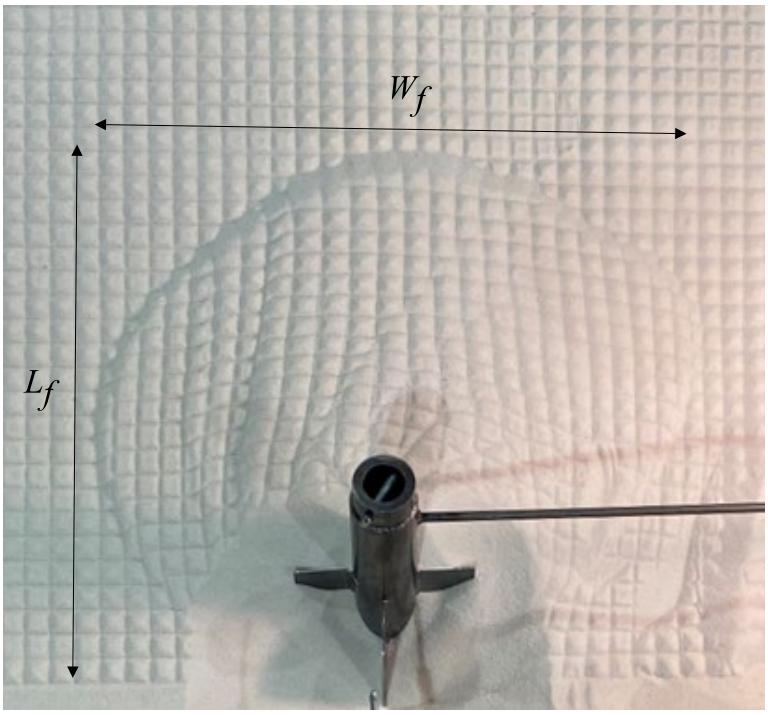

Figure 4.8. Distorted grid showing the length and width of failure wedge at a normalized lateral displacement of 1.5 for SFPF tested in dense sand deposits.

Abongo (2019) noted that the length of the influence zone is dependent on the pile head displacement and increased with an increase in lateral pile movement. Therefore, in this study, the normalized length/width of the strain wedge, i.e., the ratio of length/width of strain wedge to the pile diameter, was plotted as a function of normalized pile head displacement. Results are reported for SFPF tests in medium dense and dense sand deposits and for unfinned pile tested in dense specimen. Figure 4.9 shows the normalized strain wedge length plotted as a function of normalized pile head displacement. As Abongo (2019) used SFPF and unfinned piles with similar dimensions, a direct comparison of the results is possible. Figure 4.10 shows the comparison of the normalized strain wedge width plotted as a function of normalized pile head displacement.

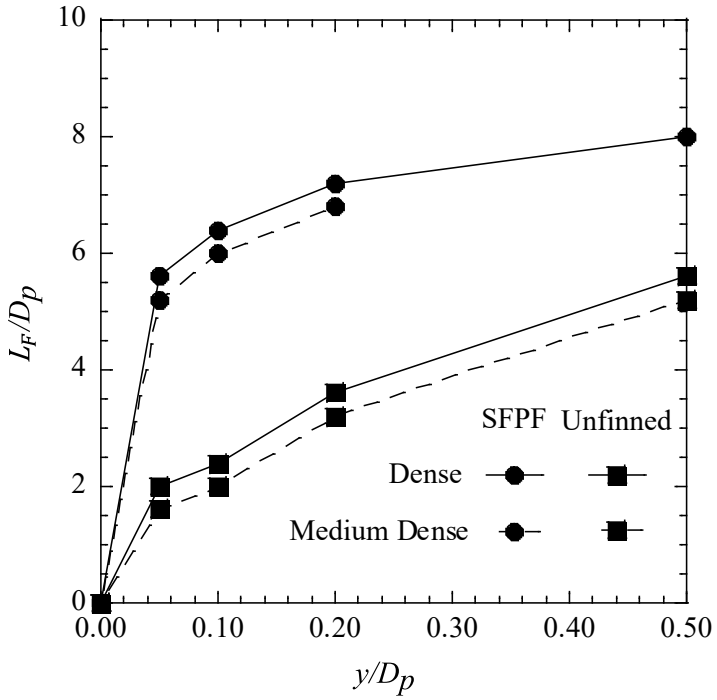

Figure 4.9. Length of failure wedge versus normalized lateral displacement for different piles and sand densities.

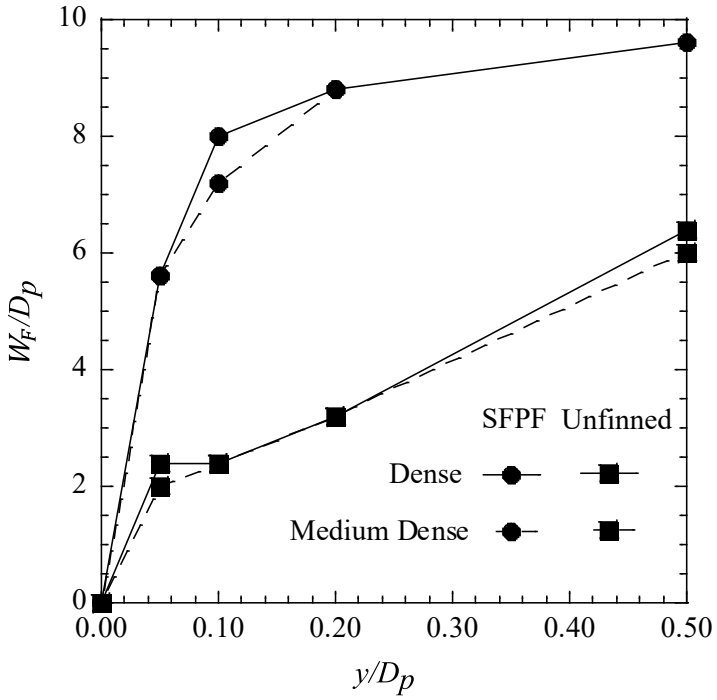

Figure 4.10. Width of failure wedge versus normalized lateral displacement for different piles and sand densities.

Figures 4.9 and 4.10 suggest that initially, there is a rapid evolution of the length and width of the failure zone. However, after a normalized pile head displacement of 0.1, the increase in length and width are smaller, especially in SFPFs. The unfinned pile showed an increase in length and width of the failure zone even after 0.1 y/D_P. As expected, the length and width of the failure zone are much lower for unfinned pile compared to the SFPFs. It is also noted from Figures 4.9 and 4.10 that the effect of density on the SFPF failure zone is minimal, as the SFPFs in medium dense sand and dense sand showed similar failure zones. Therefore, it can be concluded that the improvement in performance of SFPFs during lateral loading with an increase in density can only be attributed to the enhancement of soil properties.

4.4 COMBINED LATERAL AND TORSIONAL RESISTANCE OF SFPFs

From the previous sections, it is evident that the SFPFs significantly improve the torsional and lateral load capacity compared to unfinned piles. However, for foundation structures for transportation signs and signals, both the lateral load as well as torsion can act simultaneously on the foundations. The effect of this load combination needs to be studied, as it can influence the design of these structures. In this section, test results of combined lateral plus torsional load on SFPFs in medium dense sand and dense sand are discussed. Tests were carried out with three arm lengths of 7.5 cm, 15 cm, and 30 cm. Results are reported as torque versus rotation and lateral load versus normalized pile head displacement for different arm lengths considered. In this section, a pile rotation of 3° is considered as failure and the corresponding torque versus rotation for different arm lengths in medium dense and dense sand are shown in Figures 4.11 and 4.13. The benchmark case of pure torsional loading in these sands is also plotted in Figures 4.11 and 4.13. The corresponding lateral load versus normalized displacements are shown in Figures 4.12 and 4.14.

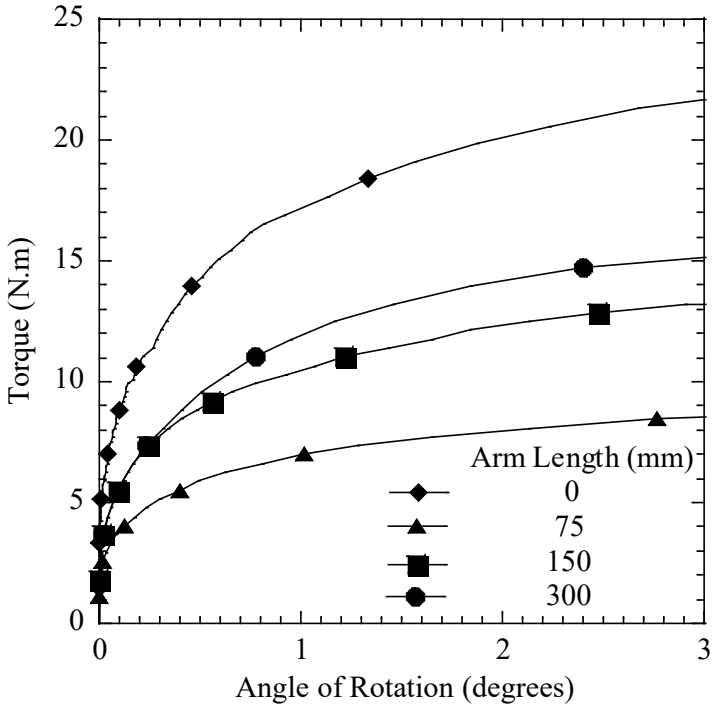

Figure 4.11. Torsion versus rotation for different arm lengths of the SFPF in medium dense sand.

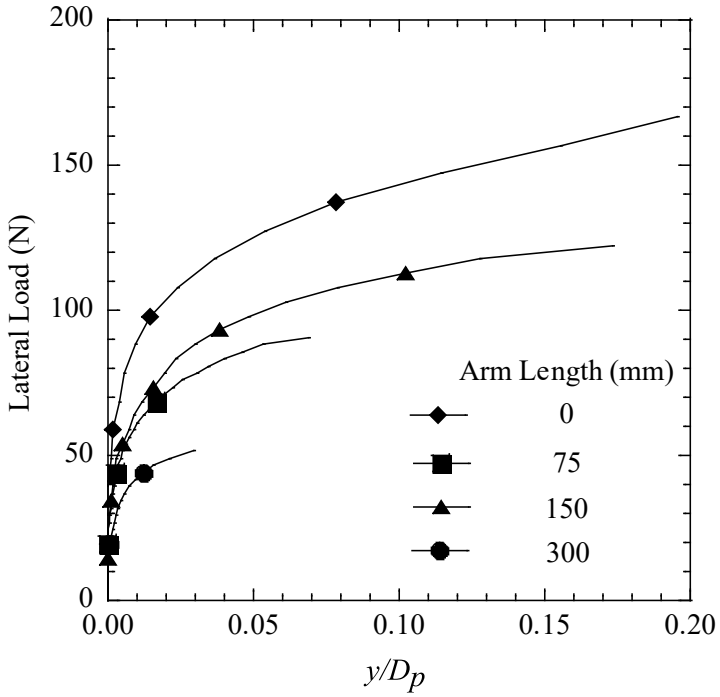

Figure 4.12. Lateral load versus normalized lateral displacement for different arm lengths of the SFPF in medium dense sand.

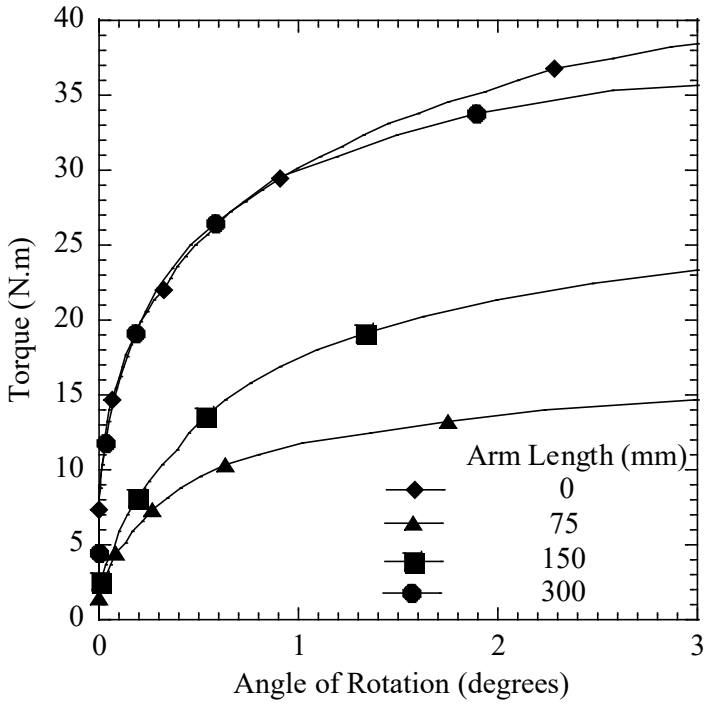

Figure 4.13. Torsion versus rotation for different arm lengths of the SFPF in dense sand.

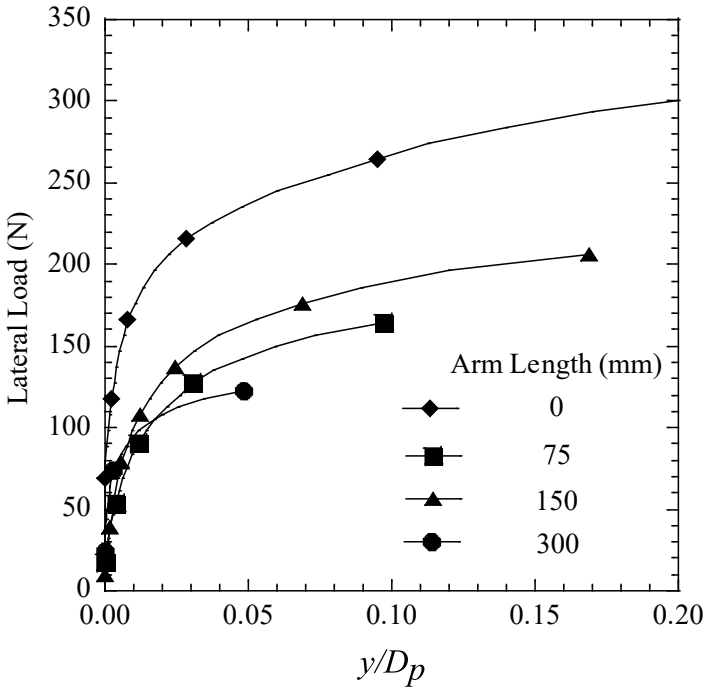

Figure 4.14. Lateral load versus normalized lateral displacement for different arm lengths of the SFPF in dense sand.

If a limiting criterion of 0.2 y/D_P used by Abongo (2019) is considered in the lateral load tests, it can be noted from Figures 4.11, 4.12, 4.13, and 4.14 that for the arm lengths greater than zero considered in this study, all the SFPFs fail in torsion. The effect of lateral loading is evident in Figure 4.9, as an increase in arm length (not considering arm length of 0) increases the torsional capacity of the SFPFs. However, Figure 4.10 shows that an increase in arm length reduces the lateral load carried by the SFPFs. For the same normalized lateral displacement considered, the SFPF loaded at an arm length of 30 cm had the lowest lateral load, followed by SFPFs with 15-cm and 7.5-cm arm lengths. The SFPF loaded with zero eccentricity (pure lateral loading) provided the highest load-carrying capacity. Figures 4.15 and 4.16 show the failure modes of the SFPF during combined loading for arm lengths of 30 cm and 7.5 cm, respectively. It is evident from Figures 4.15 and 4.16 that the lateral displacement is higher in SFPFs loaded with shorter arm length compared to SFPF loaded with longer arm length.

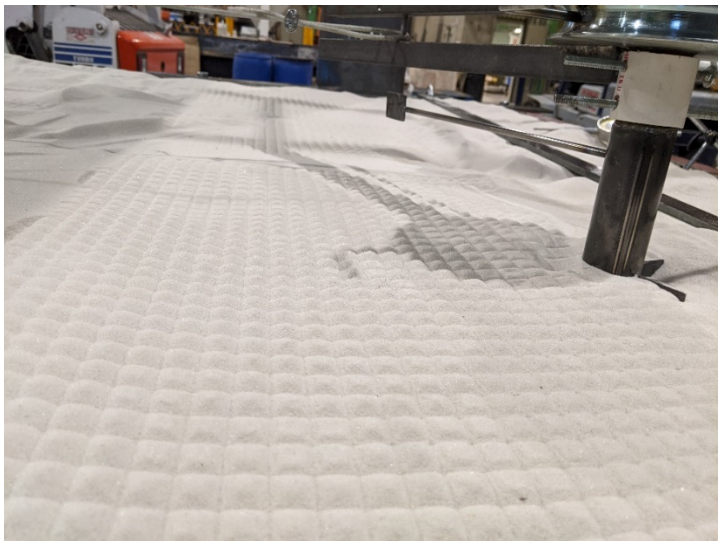

Figure 4.15. SFPF at failure during combined torsional plus lateral loading - arm length 30 cm in medium dense sand.

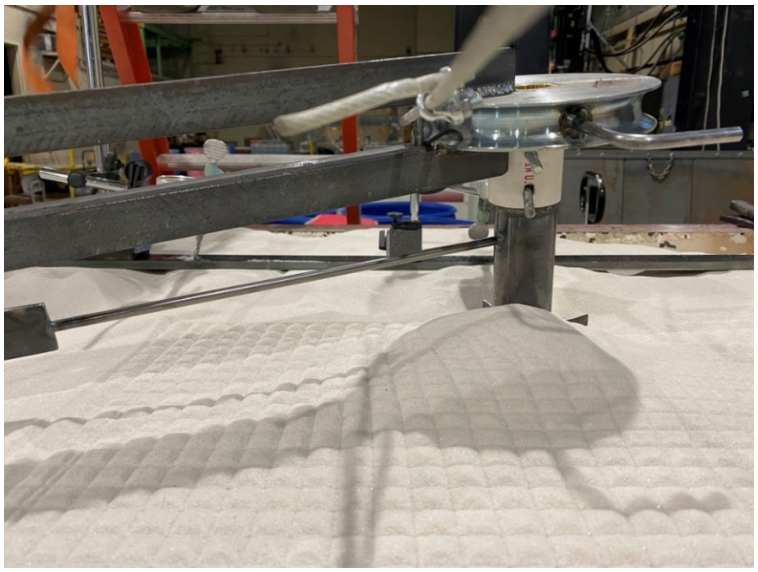

Figure 4.16. SFPF at failure during combined torsional plus lateral loading - arm length 7.5 cm in medium dense sand.

CHAPTER 5

Findings

In the present study, 16 scaled laboratory tests were conducted on SFPFs and unfinned piles to understand the effectiveness of SFPFs during torsional loading and lateral loading. Combined lateral–torsional load tests were carried out on SFPFs to understand the influence of torsional arm length on the torsional and lateral load capacities. The laboratory tests on torsional loading were carried out in dry sand at three relative density ranges of 20-30%, 45-55%, and 75-85%, typical for loose, medium dense, and dense sand, respectively. Tests on lateral loadings were carried out in medium dense and dense sand to understand the effect of steel fins and sand density on the lateral load capacity and influence zone of SFPFs and unfinned piles. The combined lateral and torsional capacity tests were also carried out in medium dense and dense sand. Based on the literature survey, optimum fin dimensions providing efficient lateral load capacity were used in the present study. The pile length to diameter ratio ($L_p/D_p = 9$), fin width to pile diameter ($W_F/D_P = 1$), and fin configuration (four-fin configuration) of the SFPFs were constant for the present study and determined on the basis of a comprehensive review of the published literature.

Based on the study design, a scaled laboratory study was implemented. Detailed explanation of the test setup, engineering drawings, and laboratory test setup photographs are provided in this report. Sand deposits were prepared using the rainfall method at selected relative density ranges. The pile installation sequences adopted in the laboratory are also discussed in detail. Results are reported in terms of torque versus rotation angle for torsional load tests and lateral load versus normalized displacement for lateral load tests. For combined lateral-torsional tests, results are reported in terms of torque versus rotation and lateral load versus normalized displacement.

Based on the laboratory test results, the following conclusions were drawn:

- The study showed the repeatability of the tests, signifying the validity of the pluviation method in obtaining uniformly deposited sand.
- The introduction of fins significantly increases the torsional capacity of the foundations. Failure in unfinned piles is caused by slippage at small angles of rotation, while the SFPFs fail at larger rotation angles. Unlike unfinned piles, torsional failure in SFPFs occurred gradually.
- Torsional capacities of both unfinned piles and SFPFs increase with an increase in sand relative density.
- The torsional efficiency of SFPFs increases with an increase in sand relative density and rotation angle.
- Lateral load tests on SFPFs and unfinned piles show that the introduction of fins increases the lateral load capacity of unfinned piles. Lateral load capacity of unfinned piles and SFPFs increases with an increase in sand relative density.
- Lateral load efficiency is highest at low lateral displacement, irrespective of the sand relative density, and decreases with an increase in lateral displacement. The lateral load efficiency of the piles is highest in medium dense sand compared to dense sand.
- Length and width of the influence zones for both unfinned piles and SFPFs increase with an

increase in lateral pile displacement. The influence zones of SFPFs are wider and longer compared to unfinned piles. The zone of influence is dependent on the pile type (SFPF or unfinned) but independent of the sand relative density.

- Combined lateral-torsional testing on SFPF shows that an introduction of arm length reduces the lateral load capacity compared to the case without any torsional load. For a certain lateral pile displacement considered, the lateral load decreases with an increase in arm length.
- The reduction in lateral load capacities with the introduction of arm length in the combined lateral-torsional testing is evident in both medium dense and dense sands.

CHAPTER 6

Recommendations

In this study, torsional, rotational, and combined torsional and rotational tests were carried out on monopiles and SFPFs in sand at different deposit densities. Based on the laboratory test results, the following recommendations are provided by the authors.

- Laboratory tests with different proportions and dimensions are recommended to understand the influence of SFPF dimensions on the torsional and lateral load capacities.
- The effectiveness of SFPFs in increasing the torsional, lateral, and combined torsional and lateral load capacities in clay is relatively unknown. Therefore, additional laboratory study of SFPFs in clay deposits to better understand the effectiveness of SFPFs in clays is recommended.
- Well-instrumented field tests are recommended to further understand the effectiveness of fins in increasing the torsional and lateral load capacities. Field tests with different moment arms will be particularly useful to understand the influence of moment on lateral load capacity and vice-versa.
- The laboratory test results can be used to calibrate numerical models. The calibrated numerical model can be used to derive analytical solutions for torsional and lateral load capacities of SFPFs as a function of pile dimensions and sand deposit density.

References

1. Abongo, K. O. (2019). "Model Study of the Static and Cyclic Lateral Capacity of Finned Piles." Ph.D. Dissertation. Lehigh University.
2. Babu, K. V., and Viswanadham, B. V. S. (2018). "Numerical Studies on Lateral Load Response of Fin Piles." *Geomechanics and Geoengineering*, 14(2), 1-14.
3. Bizaliele, M. M. (1992). "Torsional Cyclic Loading Response of a Single Pile in Sand." Ph.D. Thesis, Schriftenreihe des Instituts fur Grundbau, Ruhr-Univ., Bochum, Germany.
4. Dührkop, J., and Grabe, J. (2008). "Laterally Loaded Piles with Bulge," *Journal of Offshore Mechanics and Arctic Engineering*, ASME, 130(4), 041602.
5. Dutt, R.N. (1976). "Torsional Response of Piles in Sand." Ph.D. Thesis, University of Houston, Houston, Texas.
6. Dutt, R. N., and O'Neill, M. W. (1983). "Torsional Behavior of Model Piles in Sand." *Geotechnical Practice in Offshore Engineering*, ASCE, New York, 315-334.
7. Fleming, W.G.K., Weltman, A.J., Randolph, M.F. and Elson, W.K. (1992). *Piling Engineering* (2nd ed). Blackie Academic & Professional, Glasgow.
8. Franke, E., and Muth, G. (1985). "Scale Effect in 1g Model Tests on Horizontally Loaded Piles." In *Proceedings of the 11th International Conference of Soil Mechanics and Foundations, San Francisco*, 2, 1011–1014.
9. GAI Consultants, Inc. (1982). *The Steel Pile, Pile Cap Connection*. American Iron and Steel Institute, Washington, D.C.
10. Hajialilue-Bonab, M., Sojoudi, Y., and Puppala, A. J. (2013). "Study of Strain Wedge Parameters for Laterally Loaded Piles." *International Journal of Geomechanics,* 13(2), 143–152.
11. Hu, Z. (2003). "Determining the Optimum Depth of Drilled Shafts Subject to Combined Torsion and Lateral Loads in Saturated Sand from Centrifuge Testing." Master's Thesis, University of Florida, Gainesville, FL.
12. Hu, Z., McVay, M., Bloomquist, D., Herrera, R., and Lai, P. (2006). "Influence of Torque on Lateral Capacity of Drilled Shafts in Sands." *J. Geotech. Geoenviron. Engng*., ASCE, 132(4), 456–464.
13. Kramer, C. A., Ghasemi-Fare, O., and Basu, P. (2014). "Laboratory Thermal Performance Tests on a Model Heat Exchanger Pile in Sand." *Geotech Geol Eng.,* 33, 1–19.
14. Laue, J. and Sonntag, T. (1998). "Pile Subjected to Torsion." *Proceedings of Centrifuge, Balkema, Rotterdam, the Netherlands*, 187–192.
15. Lee, J., Kim, M., and Kyung, D. (2010). "Estimation of Lateral Load Capacity of Rigid Short Piles in Sands Using CPT Results." *J. Geotech. Geoenviron. Eng.*, 136(1), 48–56.
16. Meyerhof, G. G., Mathur, S. K., and Valsangkar, A. J. (1981). "Lateral Resistance and Deflection of Rigid Walls and Piles in Layered Soils." *Can. Geotech. Journal*, 18, 159–70.
17. McVay, M. C., Bloomquist, D., and Thiyyakkandi, S. (2014). *Field Testing of Jet-Grouted Piles and Drilled Shafts*, Report BD75-977-41, 91977. Florida Department of Transportation, Tallahassee, FL.
18. Murphy, G., Doherty, P., Cadogan, D., and Gavin, K. (2016). "Field Experiments on Instrumented Winged-monopiles," *Proceedings of the Institution of Civil Engineers-Geotechnical Engineering,* 169(3), 227-239.

19. Nasr, A. M. (2013). “Experimental and Theoretical Studies of Laterally Loaded Finned Piles in Sand.” *Canadian Geotechnical Journal*, 51(4), 381–393.
20. Peng, J. R., Rouainia, M., and Clarke, B. G. (2010). “Finite Element Analysis of Laterally Loaded Fin Piles,” *Computers and Structures*, 88, 1239-1247.
21. Poulos, H. G. (1975). “Torsional Response of Piles.” *Journal of the Geotechnical Engineering Division*, 101(10), 1019-1035.
22. Prasad, Y. V. S. N., and Chari, T. R. (1999). “Lateral Capacity of Model Rigid Piles in Cohesionless Soils.” *Soils and Foundations*, 39(2), 21-29.
23. Randolph, M. F. (1983). “Design Consideration for Offshore Piles.” *Geotechnical Practices in Offshore Engineering*, ASCE, Austin, 422–439.
24. Rutledge, P. C. (1956): Design monographs for pole structure.
25. Stoll, U. W. (1972). “Torque Shear Test of Cylindrical Friction Piles.” *Civil Engineering*, 42(4), 63-65.
26. Tawfiq, K. (2000). *Drilled Shafts Under Torsional Loading Conditions*, Report No. B-9191, Florida Department of Transportation, Tallahassee, FL.
27. Thiyyakkandi, S., McVay, M., Lai, P., and Herrera, R. (2016). “Full-scale coupled torsion and lateral response of mast arm drilled shaft foundations.” *Can. Geotech. J.*, 53 (12), 1928–1938.
28. TRB (2011). “Design Guidelines for Increasing the Lateral Resistance of Highway-Bridge Pile Foundations by Improving Weak Soils.” NCHRP Report 697.
29. Zhang, L. M., and Kong, L. G. (2006). “Centrifuge Modeling of Torsional Response of Piles in Sand.” *Canadian Geotechnical Journal*, 43(5), 500-515.